Published in final edited form as:

Nat Metab. 2024 December ; 6(12): 2300–2318. doi:10.1038/s42255-024-01162-0.

Cryptic phosphoribosylase activity of NAMPT restricts the virion incorporation of viral proteins

Shu Feng[1,5,6], **Na Xie**[1,2,6], **Yongzhen Liu**[1], **Chao Qin**[1], **Ali Can Savas**[1], **Ting-Yu Wang**[1,3], **Shutong Li**[1], **Youliang Rao**[1], **Alexandra Shambayate**[1], **Tsui-Fen Chou**[3], **Charles Brenner**[4], **Canhua Huang**[2], **Pinghui Feng**[1,✉]

[1]Section of Infection and Immunity, Herman Ostrow School of Dentistry, Norris Comprehensive Cancer Center, University of Southern California, Los Angeles, CA, USA.

[2]State Key Laboratory of Biotherapy and Cancer Center, West China Hospital and West China, School of Basic Medical Sciences & Forensic Medicine, Sichuan University, and Collaborative Innovation Center for Biotherapy, Chengdu, PR China.

[3]Proteome Exploration Laboratory, Beckman Institute, California Institute of Technology, Pasadena, CA, USA.

[4]Department of Diabetes and Cancer Metabolism, Beckman Research Institute, City of Hope, Duarte, CA, USA.

[5]Present address: Department of Diabetes and Cancer Metabolism, Beckman Research Institute, City of Hope, Duarte, CA, USA.

[6]These authors contributed equally: Shu Feng, Na Xie.

Abstract

As obligate intracellular pathogens, viruses activate host metabolic enzymes to supply intermediates that support progeny production. Nicotinamide phosphoribosyltransferase (NAMPT), the rate-limiting enzyme of salvage nicotinamide adenine dinucleotide (NAD^+) synthesis, is an interferon-inducible protein that inhibits the replication of several RNA and DNA viruses through unknown mechanisms. Here, we show that NAMPT restricts herpes simplex virus type 1 (HSV-1) replication by impeding the virion incorporation of viral proteins

✉**Correspondence and requests for materials** should be addressed to Pinghui Feng. pinghuif@usc.edu.

Author contributions

P.F. and S.F. conceived the project. S.F., N.X., Y.L., C.Q., T.W., P.F. and T.C. determined the methodology. S.F., N.X., Y.L., C.Q., A.C.S., T.W., Y.R., S.L. and A.S. performed the investigation. P.F., C.B. and C.H. acquired funding. P.F. and C.H. were responsible for project administration. P.F., C.B., C.H. and T.C. supervised the project. P.F. and S.F. wrote the original draft of the manuscript; P.F., S.F., C.B. and C.Q. reviewed and edited the final version.

Reporting summary

Further information on research design is available in the Nature Portfolio Reporting Summary linked to this article.

Competing interests

C.B. is a chief scientific advisor of ChromaDex and co-founder of Alphina Therapeutics. P.F. is a consultant for Marc J Bern & Partners. All other authors declare no competing interests.

Extended data is available for this paper at https://doi.org/10.1038/s42255-024-01162-0.

Supplementary information The online version contains supplementary material available at https://doi.org/10.1038/s42255-024-01162-0.

owing to its phosphoribosyl-hydrolase (phosphoribosylase) activity, which is independent of the role of NAMPT in NAD^+ synthesis. Proteomics analysis of HSV-1-infected cells identifies phosphoribosylated viral structural proteins, particularly glycoproteins and tegument proteins, which are de-phosphoribosylated by NAMPT in vitro and in cells. Chimeric and recombinant HSV-1 carrying phosphoribosylation-resistant mutations show that phosphori bosylation promotes the incorporation of structural proteins into HSV-1 virions and subsequent virus entry. Loss of NAMPT renders mice highly susceptible to HSV-1 infection. Our work describes an additional enzymatic activity of a metabolic enzyme in viral infection and host defence, offering a system to interrogate the roles of protein phosphoribosylation in metazoans.

Viruses are obligate intracellular pathogens that rely on cellular machinery for the synthesis of diverse macromolecules that collectively support viral replication. Not surprisingly, viruses often activate cellular metabolic enzymes to fuel viral replication, presumably by providing metabolites for the synthesis of viral structural building blocks[1]. Indeed, interferon (IFN)-inducible enzymes that interfere with metabolites that are essential for viral replication can function to restrict the infection of distinct viruses, thus acting as effectors within the broad IFN response network[2,3]. For example, SAMHD1 hydrolyzes deoxyribonucleoside triphosphate to limit human immunodeficiency virus (HIV) replication in nonpermissive cells, and viperin catalyses the synthesis of 3′-deoxy-3′,4′-didehydro-cytidine triphosphate, which terminates the RNA-dependent RNA polymerization of diverse RNA viruses[4,5]. Cholestrol-25-hydroxylase (CH25H) converts cholesterol into 25-hydroxylcholesterol, which inhibits the membrane fusion between cells and envelope viruses[6]. These studies illustrate a paradigm that IFN-inducible metabolic enzymes restrict viral replication through their metabolites. How other IFN-inducible metabolic enzymes act to combat viral infection is not well understood.

NAD^+ is a vital enzyme cofactor in all living cells[7]. NAD^+ homoeostasis is maintained by a balance between its synthesis and consumption. NAD^+ is consumed chiefly by NAD^+-dependent enzymes, such as polyADP-ribose polymerases (PARPs) and sirtuin deacetylases (SIRTs), and by glycohydrolases such as CD38 and sterile alpha and toll/interleukin receptor motif-containing protein 1 (SARM1), yielding nicotinamide (NAM) as a byproduct[8,9]. Protein ADP-ribosylation and polyADP-ribosylation have critical roles in diverse biological processes including gene expression, DNA damage response and translation[10-12]. Although the phosphoribose of proteins can be processed from ADP-ribose and polyADP-ribose by nudix hydrolase 16 (NUDT16), ectonucleotide pyrophosphatase/phosphodiesterase 1 (ENPP1) or snake venom phosphodiesterase (svPDE) in vitro[13,14], the biogenesis and roles of phosphoribosyl moieties on proteins are poorly understood in metazoans. NAM is converted into nicotinamide mononucleotide (NMN) by NAMPT, the rate-limiting enzyme of the salvage NAD^+ synthesis, to regenerate NAD^+. The pivotal roles of NAMPT in diverse biological processes are reflected by its upregulation in microbial infection and cancer cells as well as its deficiency in neurodegenerative diseases[9,15,16]. Previous studies have implicated NAMPT in antiviral defence against diverse viruses, including HIV, yellow fever virus and mouse cytomegalovirus, although its mechanism of action remains uncharacterized. Here, we report that NAMPT exerts antiviral activity against HSV-1 independent of its activity in NAD^+ synthesis. Surprisingly, NAMPT directly

de-phosphoribosylates viral structural proteins, thereby impeding HSV-1 virion assembly and entry of subsequent infection.

Results

NAMPT restricts HSV-1 lytic replication independent of NAD^+

By analysing metabolites of HSV-1-infected cells, we found that HSV-1 significantly depletes NAD^+ and its related metabolites, such as NADH, $NADP^+$ and NAM, during lytic replication (Fig. 1a and Extended Data Fig. 1a). In mammalian cells, NAD^+ is often rapidly replenished through the activity of the rate-limiting NAMPT of the salvage pathway (Fig. 1b). Thus, we depleted key enzymes responsible for NAD^+ synthesis, including NAMPT, nicotinamide riboside kinase (NRK), NMN adenylyltransferase 1 (NMNAT1) and NAD^+ synthetase (NADSYN), by short hairpin RNA-mediated knockdown and examined HSV-1 lytic replication (Fig. 1b). Surprisingly, depletion of NAMPT, but not the other three enzymes, increased the extracellular HSV-1 titre (Fig. 1c,d). Transient depletion of all four enzymes had no effect on cell viability (Extended Data Fig. 1b). Similarly, depletion of NAMPT also increased HSV-1 lytic replication in HepG2 cells (Fig. 1e). These results suggest that NAMPT is antiviral against HSV-1.

NAMPT is crucial for intracellular NAD^+ regeneration. Indeed, mass spectrometry analysis showed that NAMPT depletion reduced intracellular NAD^+ and NMN in mock-infected and HSV-1-infected HeLa cells by 50% (Extended Data Fig. 1c). Addition of nicotinamide riboside (NR), but not nicotinic acid, increased intracellular NMN and NAD^+ levels in a dose-dependent manner (Extended Data Fig. 1c,d-f). The dose-dependent effect of exogenous NR to restore intracellular NAD^+ was confirmed in mock-infected and HSV-1-infected single-guide RNA targeting NAMPT (sgNAMPT) HeLa cells (Extended Data Fig. 1f). The increase in intracellular NR and NMN by NR supplementation was more pronounced in HSV-1-infected cells than in mock-infected cells. NR restored intracellular NAD^+ of NAMPT-knockout (KO) cells to that of wild-type HeLa cells at 0.1 mM (Extended Data Fig. 1f). We then supplemented NAMPT-depleted HeLa cells with NR (0.1 mM) and found that addition of NR further boosted HSV-1 lytic replication in NAMPT-depleted HeLa cells (Extended Data Fig. 1g), as shown by extracellular and intracellular HSV-1 titres (Fig. 1f and Extended Data Fig. 1h). Conversely, ‘reconstituted’ expression of NAMPT reduced HSV-1 lytic replication in NAMPT-KO cells (Extended Data Fig. 2a). Moreover, FK866, an inhibitor of NAMPT as validated by an in vitro NAD^+ synthesis assay, reduced HSV-1 lytic replication in HepG2 cells and addition of NR restored HSV-1 replication, whereas addition of NR had no effect on HSV-1 replication in dimethylsulfoxide-treated cells (Extended Data Fig. 2b,c). Similarly, NAMPT knockdown increased HSV-1 lytic replication in human HepG2 cells (Extended Data Fig. 2d). Furthermore, the expression of exogenous NAMPT in 293T cells reduced HSV-1 replication in a dose-dependent manner (Extended Data Fig. 2e). Finally, the depletion of NAMPT in mouse embryonic fibroblasts and human foreskin fibroblasts, primary cells from mice and humans, significantly increased HSV-1 lytic replication, as determined by the extracellular HSV-1 (Extended Data Fig. 2f,g). Thus, NAMPT reduces HSV-1 lytic replication independent of its activity in NAD^+ synthesis.

NAMPT restricts HSV-1 lytic replication independent of phosphoribosyl-pyrophosphate

In addition to salvaging NAD^+ synthesis, NAMPT consumes phosphoribosyl-pyrophosphate (PRPP), which may be a limiting factor for HSV-1 replication. We first measured the level of PRPP in control and NAMPT-KO cells. Deletion of NAMPT increased the intracellular PRPP, whereas addition of NR had no effect on PRPP levels and consistently increased HSV-1 lytic replication (Fig. 1g). We then manipulated intracellular PRPP levels by over-expressing nicotinic acid phosphoribosyltransferase (NAPRT), silencing uracil phosphoribosyltransferase (UPRT, also known as UMP synthetase) or supplementing NAM and examined HSV-1 lytic replication (Extended Data Fig. 2h,i). NAPRT catalyses the Preiss–Handler pathway using nicotinic acid and PRPP as substrates, and UPRT adds phosphoribosyl moiety to uracil to synthesize UMP. Thus, NAPRT overexpression and UPRT depletion are expected to decrease or increase intracellular PRPP levels, respectively. Indeed, NAPRT expression decreased PRPP by ~90% in mock-infected HeLa cells, and it had no effect on HSV-1 replication (Fig. 1h). Conversely, a ~35% reduction in UPRT mRNA levels increased PRPP by threefold and demonstrated no effect on HSV-1 replication (Fig. 1i). NAM supplementation did not significantly alter intracellular PRPP and HSV-1 replication (Extended Data Fig. 2j). Thus, NAMPT restricts HSV-1 lytic replication independent of intracellular NAD^+ and PRPP levels.

NAMPT is antiviral against HSV-1 in mice

To probe the in vivo role of NAMPT in HSV-1 infection, we induced NAMPT deletion with tamoxifen in conditional NAMPT-KO mice (*Nampt*$^{flox/flox}$*:cre*) that were bred from *Nampt*^{tm10leo}/ImaiJ and B6;129-*Gt(ROSA)26Sor*$^{tm1(cre/ERT2)Tyj}$/J. When the mice were treated with tamoxifen, we found that NAMPT depletion was apparent in the liver and spleen but not detectable in the brain, kidney, heart, and lung (Fig. 2a and Extended Data Fig. 3a). At the time of HSV-1 infection, wild-type and NAMPT-KO mice demonstrated no significant difference in body weight (Extended Data Fig. 3b). When mice were infected with a sublethal dose of HSV-1 (5×10^7 plaque-forming units (PFU)) by intravenous injection that enables synchronized and systemic infection, we found that 90% of NAMPT-KO mice succumbed to HSV-1 infection by day 6 post infection, whereas 70% of wild-type mice survived HSV-1 infection under the same conditions (Fig. 2b). Consistent with this observation, haematoxylin and eosin (H&E) staining revealed localized tissue destruction throughout the liver of NAMPT-KO mice but not in that of wild-type mice (Fig. 2c and Extended Data Fig. 3c). Immunohistochemical staining showed that HSV-1 lytic antigens, including UL37 and UL47, were readily detected in areas with tissue destruction (Fig. 2c and Extended Data Fig. 3c). The HSV-1 load in the livers of NAMPT-KO mice was four orders of magnitude higher in viral titre and two orders of magnitude hinger in genome copy number than that in wild-type mice (Fig. 2d,e). Taken together, NAMPT demonstrates antiviral activity against HSV-1 in cells and in mice.

To assess whether exogenous NR increases HSV-1 replication in mice as it did in cultured cells, we performed NR intraperitoneal injections (400 mg kg^{-1} d^{-1}) in NAMPT-KO mice starting at the time of tamoxifen induction. We then examined mouse survival, NAD^+-related metabolites and HSV-1 replication in the liver where NAMPT had been depleted (Fig. 2f). Liquid chromatography-mass spectrometry (LC–MS) analysis showed that loss of

NAMPT reduced NAD^+ levels by ~50% in the liver (Fig. 2g). This reduction was restored to the level found in the livers of wild-type mice by exogenous NR administration, and these mice had similar body weights (Extended Data Fig. 3d). Considering that NR may increase HSV-1 replication, we infected mice with a dose (2×10^7 PFU) lower than the sublethal dose of HSV-1 and monitored mouse survival. We found that 40% and 70% of NAMPT-KO mice succumbed to HSV-1 infection by day 4 and day 12, respectively, whereas no wild-type mice died from HSV-1 infection (Fig. 2h). Remarkably, 90% of NAMPT-KO mice that received NR injection succumbed to HSV-1 infection by day 7 post infection. The plaque assay showed that the loss of NAMPT increased HSV-1 lytic replication by two orders of magnitude, and this effect was further elevated by ~50-fold with NR supplementation (Fig. 2i). The increased HSV-1 titre also correlated with a similar pattern of viral lytic gene expression, as analysed by real-time PCR (Fig. 2j). HSV-1 was not detected in the spleen of either wild-type or NAMPT-KO mice, supporting the hepatocyte-intrinsic antiviral activity of NAMPT. These results collectively show that NAMPT restricts HSV-1 lytic replication in mice independent of NAD^+ synthesis.

NAMPT-deficient mice mount a normal innate immune response

Immune defence is critical for HSV-1 lytic replication, and NAMPT depletion may compromise the host's antiviral immune response against HSV-1. To determine whether the loss of NAMPT compromises host antiviral immune defence, we examined the expression of inflammatory genes in NAMPT-deleted cultured cells and mice upon HSV-1 infection. We found that NAMPT deletion in HeLa and HepG2 cells did not significantly decrease the expression of inflammatory genes, represented by *IFNb*, *ISGs* and *IRF7* (Extended Data Fig. 4a-c). Furthermore, real-time PCR analysis showed that in response to HSV-1 infection, most inflammatory genes, such as *Ifnb*, *Tnf*, *Isg*s and *Il6*, were expressed without significant difference in the liver of wild-type and NAMPT-KO mice. Although *Ifnb* and *Isg56* were expressed at slightly lower levels in mock-infected NAMPT-KO mice regardless of NR supplementation, the induction was minimal, and the difference was diminished by HSV-1 infection (Extended Data Fig. 4d). Interestingly, the expression of two chemokines, *Cxcl1* and *Cxcl2* (*Mip2*), was significantly higher in the liver of NAMPT-KO and NAMPT-KO supplemented with NR than in wild-type mice with HSV-1 infection. This pattern was similar to the increased expression of *Cxcl1* observed even without HSV-1 infection (Extended Data Fig. 4d). These results collectively support the conclusion that loss of NAMPT does not compromise host antiviral innate immune response against HSV-1.

Evidence that NAMPT acts on HSV-1 tegumentation in the trans-Golgi network

NAMPT localizes to diverse subcellular compartments within mammalian cells, including the cytosol, nucleus, mitochondrion, endoplasmic reticulum and trans-Golgi network (TGN)[17]. To enable NAMPT detection by immunofluorescence and immunogold staining, we used sgNAMPT HeLa cells that were reconstituted with HA–NAMPT expression. Upon HSV-1 infection, we observed redistribution of NAMPT with the progression of HSV-1 lytic replication. Specifically, NAMPT was enriched and localized to the perinuclear region as punctate structures at late stages of infection. Further immunofluorescence staining showed that these punctate structures were positive for NAMPT, UL19 and TGN46 (Fig. 3a). These vesicular structures extended to regions proximal to the plasma membrane, suggesting that

these vesicles containing HSV-1 virions were probably en route to the plasma membrane for release. NAMPT was also observed to colocalize with glycoprotein B (gB) and the UL19 major capsid protein in structures reminiscent of the TGN, which is the compartment in which glycoproteins and tegument proteins are packaged into virion particles (Extended Data Fig. 5a)[18]. We further examined the interaction of NAMPT with HSV-1 assembly and egress processes by electron microscopy. In subcellular compartments that were positive for TGN46, double-membrane structures containing HSV-1 virions were observed and NAMPT was localized to the outer membrane (Fig. 3b, left top panel). An invaginating virion within the TGN was detected through immunostaining, revealing that NAMPT and TGN46 were found at two separate ends of the unclosed membrane structure (Fig. 3b, left bottom panel). NAMPT was also detected in proximity to virions within the lumen of the double-layered membrane structure, which is localized in the vicinity of TGN stacks (Fig. 3b, right panel and Extended Data Fig. 5b,c). As shown in Fig. 3c, the presence of HSV-1 virions in the lumen of the TGN was further confirmed through staining for UL19 and NAMPT. Within a subcellular compartment where a vesicle containing HSV-1 virions was pinching from the membrane, abundant NAMPT was detected at the site of membrane closure (Fig. 3c, left panel). These observations provide temporal and spatial information regarding the action of NAMPT during HSV-1 lytic replication. We also detected subcellular regions that were stained predominantly for NAMPT and UL19 (Fig. 3c, right panel). These results collectively support the conclusion that NAMPT acts within proximity of the TGN to restrict HSV-1 progeny assembly.

We then determined whether NAMPT is associated with HSV-1 virions. First, NAMPT was detected in fractions containing HSV-1 virions analysed by sucrose gradient centrifugation and immunoblotting for viral structural components, including UL19, gB, gD, UL37 and VP16 (Fig. 3d). These fractions were devoid of exosomes detectable with antibodies to well-established exosome markers, including CD9, CD81, Alix and CD63 (Fig. 3d and Extended Data Fig. 5d). Using purified HSV-1 virions, we performed immunogold staining and found that NAMPT was abundantly detected in proximity to UL19 of HSV-1 capsids (Fig. 3e and Extended Data Fig. 5e). Interestingly, some virions showed little or no NAMPT staining, probably because of the incomplete permeabilization by NP-40, and measured ~150–200 nm in diameter, which is consistent with the size of enveloped HSV-1 virions[19]. When treated with proteinase K, virion-associated NAMPT was resistant to proteinase K without detergent but became sensitive to proteinase K upon treatment with Triton X-100, demonstrating a sensitivity pattern similar to that of UL19 and UL37, which are capsid and tegument proteins packaged within the membrane, respectively (Extended Data Fig. 5f). To test whether NAMPT can associate with de-enveloped HSV-1 nucleocapsids, we performed a co-sedimentation experiment using sucrose ultracentrifugation as previously reported[20]. We found that de-enveloped, but not intact HSV-1 virions, precipitated exogenous NAMPT purified from bacteria during ultracentrifugation (Fig. 3f). These results show that NAMPT is packaged in the tegument compartment of HSV-1 virions.

To identify the viral proteins with which NAMPT interacts, we conducted ascorbic acid peroxidase (APEX)-mediated proximity labelling, biotin-based protein purification and mass spectrometry analysis using HSV-1-infected HeLa cells expressing NAMPT–APEX2 (Extended Data Fig. 5g). Compared to APEX2, NAMPT–APEX2 expression resulted in the

enrichment of several structural proteins, including tegument UL37, UL47, VP22, VP16 and US2; capsid UL19 and UL38; and envelope gB, gE, gD and gM glycoproteins (Fig. 3g and Supplementary Tables 1 and 2). When co-immunoprecipitation was performed to confirm these interactions, we found that NAMPT interacts with several glycoproteins, including gB, gD and gH in HSV-1-infected HeLa cells; and with tegument proteins, including UL21, UL37, UL47, VP16 and VP22 in transfected 293T cells (Fig. 3h and Extended Data Fig. 5h,i). No interaction between NAMPT and UL19, UL38 or UL18 was detected under similar conditions (Extended Data Fig. 5j). We then purified HSV-1 virions derived from wild-type and NAMPT-KO HepG2 cells and analysed them by immunoblotting. This showed that when HSV-1 virions were normalized with the UL19 major capsid protein, higher levels of VP22, gD, gH and, to a lesser extent, gB were detected in virions produced from NAMPT-KO HepG2 cells compared to those produced from wild-type HepG2 cells (Fig. 3i). No significant change was observed for UL37. Notably, the migration of VP16 was clearly retarded by loss of NAMPT, suggesting possible post-translational modifications. Increases in VP22, gD and gB in virions produced from NAMPT-KO HepG2 cells and, to a lesser extent, from NAMPT-depleted HeLa cells were also observed (Extended Data Fig. 5k). These results demonstrate that NAMPT restricts the incorporation of tegument proteins and glycoproteins into HSV-1 virions.

NAMPT is a protein phosphoribosylase

Given that NAMPT interacts with multiple proteins and alters their incorporation into HSV-1 virions, we reasoned that this may depend on its activity to remove phosphoribosyl moieties. Inspired by previous studies demonstrating that other metabolic enzymes act on proteins post-translationally[21,22], we speculated that NAMPT catalyses the hydrolysis of phosphoribosyl moieties of viral and cellular proteins to restrict HSV-1 replication. To differentiate it from the phosphatase activity toward the phosphoribosyl moiety, we designate the glycohydrolase activity of NAMPT as a phosphoribosylase. To test this hypothesis, we reconstituted NAMPT-KO HeLa cells with wild-type NAMPT or the NAMPT-H247E and NAMPT-D219A mutants that are impaired for phosphoribosyl transfer and substrate (NAM)-binding, respectively, for HSV-1 lytic replication[23]. Notably, although the NAMPT-H247E and NAMPT-D219A mutants are functionally compromised, significant residual enzyme activity could be detected by an in vitro NAD^+ synthesis assay (Extended Data Fig. 6a). Interestingly, wild-type NAMPT, but not the NAMPT-H247E mutant, inhibited HSV-1 replication (Fig. 4a and Extended Data Fig. 6b). The NAMPT-D219A mutant, however, more robustly reduced HSV-1 replication despite all three being expressed at similar levels. Thus, the enzyme activity required for NAMPT-mediated restriction of HSV-1 is distinct from its activity in the salvage NAD^+ synthesis. Next, we performed a modified phosphoproteomics protocol, consisting of phosphopeptide enrichment and LC–MS analysis to identify phosphoribosylated peptides using HSV-1-infected HeLa cells expressing the NAMPT-H247E mutant or with NAMPT deletion (sgNAMPT) (Fig. 4b). Given that the quantification of individual phosphoribosylated peptides was not technically feasible, we used the quantity of total phosphoribosylated peptides that was normalized to that of the total peptides as a proxy for phosphoribosylation efficiency. When the quantity of the total phosphoribosylated peptides was normalized to that of the total peptides, NAMPT-H247E reduced the percentage of phosphoribosylated peptides by >91% (Extended Data

Fig. 6c and Supplementary Tables 3-9). By contrast, NAMPT-H247E expression nearly doubled the percentage of the phosphoribosylated viral peptides that were normalized to the total peptides or total viral peptides. Consequently, NAMPT-H247E expression increased the percentage of the phosphoribosylated peptides in HSV-1 virions. Despite the low abundance of phosphoribosylated peptides, these results support the notion that NAMPT de-phosphoribosylates viral proteins and NAMPT-H247E acts as a dominant negative mutant of NAMPT. In total, 5,029 proteins, 31,846 peptides and 70 phosphoribosylated peptides were identified with confidence from the HSV-1-infected HeLa cells. Notable examples include 19 phosphoribosylated peptides of viral proteins, including glycoproteins gB, gD and gH; tegument proteins VP22, VP16, UL21, UL37, UL46 and UL47; and capsid proteins UL19, UL17 and UL18 (Extended Data Fig. 6d and Supplementary Tables 3 and 5-8). Interestingly, three ADP-ribosylated peptides of VP22 were identified as well. All ribosylated sites contained either phosphoribose or ADP-ribose, but not both, suggesting that phosphoribose and ADP-ribose mark distinct biochemical and functional entities of these modified peptides in HSV-1 infection. Notably, these phosphoribosylated proteins largely overlap with those NAMPT-binding partners identified by APEX2-mediated proximity labelling (Fig. 3g). Among these phosphoribosylation sites, most are aspartate or glutamate and a few are arginine, which is consistent with the profile of ADP-ribosylation and phosphoribosylation sites that have been previously reported (Fig. 4c)[24-26]. Phosphoribosylation of these viral peptides was validated by parsing the mass spectrum of each peptide (Fig. 4d and Supplementary Fig. 1; PRIDE accession no. PDX050684). Phosphoribosylated peptides of cellular proteins were identified but their roles in HSV-1 replication were not investigated in this study.

VP22, one of the most abundant tegument proteins, is highly phosphoribosylated as indicated by the multiple peptides carrying phosphoribose. We analysed the charge status of VP22 by two-dimensional gel electrophoresis with the overexpression of wild-type NAMPT or the NAMPT-H247E mutant. We found that wild-type NAMPT diminished the more negatively charged species and the NAMPT-H247E mutant abolished the more positively charged species, suggesting that NAMPT-H247E functions as a dominant negative mutant to inhibit the phosphoribosylase activity of endogenous NAMPT (Fig. 4e). Conversely, re-expression of NAMPT in NAMPT-KO 293T cells shifted VP22 toward the negative pole of the gel strip, providing support for the phosphoribosylase activity of NAMPT against VP22 (Extended Data Fig. 6e). Furthermore, purified wild-type NAMPT, but not the NAMPT-H247E mutant, released phosphoribose in an in vitro assay (Fig. 4f and Extended Data Fig. 6f,g). However, we were unable to quantify the phosphoribosylated peptides owing to their low abundance. Compared to NAMPT, the terminal ADP-ribose glycohydrolase 1 (TARG1) demonstrated higher activity, probably because of its lower substrate selectivity. When VP22 was analysed by two-dimensional gel electrophoresis, we found that wild-type NAMPT and the NAMPT-D219A mutant, but not the NAMPT-H247E mutant, shifted VP22 toward the negative end of gel strip, consistent with its phosphoribosylase activity against HSV-1 proteins (Fig. 4g). With VP22 defined as a substrate of NAMPT, we generated a VP22-E257A mutant and found that it was not shifted by the NAMPT-H247E mutant as analysed by two-dimensional gel electrophoresis, further supporting that NAMPT acts as a phosphoribosylase for VP22 (Extended Data Fig. 6h). To

further characterize the protein phosphoribosylase activity of NAMPT, we performed an in vitro assay using purified HSV-1 virions, because purified GST–VP22 was not sufficient to achieve maximal velocity (V_{max}) of the phosphoribosylase activity of NAMPT. When released phosphoribose was quantitatively determined by LC–MS, NAMPT demonstrated a V_{max} of 16.95 nmol min^{-1} mg^{-1} and a catalytic constant (K_{cat}) of 0.901 min^{-1} toward HSV-1 virions (Fig. 4h and Extended Data Fig. 6i). The V_{max} of phosphoribosylase activity of NAMPT is very close to that of its phosphoribosyltransferase activity that was previously reported[27], whereas the K_{cat} of the phosphoribosylase activity is ~30% lower than that of its phosphoribosyltransferase activity (Fig. 4i). These results collectively support the conclusion that NAMPT is a protein phosphoribosylase.

Phosphoribose promotes protein incorporation into virions

Having defined NAMPT as a protein phosphoribosylase and identified a panel of phosphoribosylated viral proteins, we then assessed the charge status of HSV-1 proteins by expressing the dominant negative NAMPT-H247E mutant. This assay showed that NAMPT-H247E expression reduced the charge of several HSV-1 proteins, including gB, gD, gH and UL21, and it had no significant effect on that of UL17 and UL38 (Extended Data Fig. 7a-f). A minor increase in charge was observed for VP16, UL18, UL19, UL37 and UL47 under similar conditions (Extended Data Fig. 7g-k). These results suggest that NAMPT potentially acts as a phosphoribosylase for multiple viral proteins.

To determine whether phosphoribosylation affects viral protein incorporation, we first analysed the charge status of gD expressed in HSV-1-infected cells and of HSV-1 virions. A total of six species with distinct charge statuses were detected for gD expressed in HSV-1-infected cells and extracellular HSV-1 virions. Interestingly, gD packaged in HSV-1 virions exhibited more negatively charged species than that expressed in HSV-1-infected cells (Extended Data Fig. 7l,m). This was reflected by the reduced abundance of the most positively charged species and a corresponding increase in the more negatively charged species of the virion-associated gD. We then analysed the effect of NAMPT-KO on the charge status of gD, and two-dimensional gel electrophoresis revealed a total of ten species of gD by charge status in HSV-1-infected cells and purified virions (Fig. 5a). In control HepG2 cells, gD packaged in HSV-1 virions was more negatively charged than that expressed in HSV-1-infected cells. Remarkably, NAMPT-KO in HepG2 cells resulted in a major shift toward gD species that were highly negatively charged in both HSV-1-infected cells and HSV-1 virions. Furthermore, the more negatively charged species were enriched in HSV-1 virions compared to those expressed in HSV-1-infected cells. Quantification of the distinct gD species showed that loss of NAMPT had a significant impact on the charge status of gD, resulting in the packaging of more negatively charged species in HSV-1 virions (Fig. 5b). These results support the conclusion that gD is probably phosphoribosylated and that highly phosphoribosylated gD species are incorporated into HSV-1 virions.

To further profile the effect of phosphoribosylation-resistant mutations on HSV-1 proteins, we generated mutant constructs of structural proteins and analysed their incorporation into HSV-1 virions. To do so, transfected 293T cells were infected with wild-type HSV-1 to collect chimeric virions that carry both wild-type and a mutant form of the structural

protein in the medium (Fig. 5c). Virion incorporation of the mutant protein was analysed by immunoblotting. When wild-type VP22 and its mutants incorporated in extracellular HSV-1 virions were normalized with the UL19 major capsid protein, we found that mutations of E77A and E257A reduced VP22 virion incorporation without affecting VP22 expression (Fig. 5d). By contrast, phosphoribosylation-resistant mutations E74A, D75A and R254A had no effect on the virion incorporation of VP22, indicating the site-specific effect of phosphoribosylation. Phosphoribosylation-resistant mutations of gB and gD reduced their incorporation in HSV-1 virions, and the mutation of gH increased its expression in transfected or infected cells and subsequent virion incorporation (Fig. 5e-g). Mutations of UL37 (E238A), VP16 (E6A, D7A, D11A and E314A), UL18 (D9A and D45A) and UL47 (E636A and D669A) had no significant effect on their virion incorporation (Extended Data Fig. 8a-d). Interestingly, UL32-E353A did not affect its own expression in cells or incorporation into HSV-1 virions, although it impeded the virion incorporation of UL37 but not VP16 (Extended Data Fig. 8e). This effect may stem from the slightly lower UL37 expression in HSV-1-infected cells. These results show that phosphoribosylation of VP22 and glycoproteins promotes their incorporation into HSV-1 virions.

Next, we engineered recombinant HSV-1 carrying mutations abolishing phosphoribosylation via bacteria artificial chromosome (BAC) and examined the virion incorporation of structural proteins (Fig. 6a and Extended Data Fig. 9a). In parallel, we also generated recombinant HSV-1 that contained mutations abolishing the ADP-ribosylation of VP22; that is, R86A, E149A and E234A (Extended Data Fig. 6d). All mutations were validated by sequencing of the targeted region of the HSV-1 genome (Extended Data Fig. 9b,c). Phosphoribosylation-resistant mutations in VP22, gB, gD and VP16 significantly reduced HSV-1 replication, whereas mutations in gH, UL17, UL37 and UL47 had no apparent effect on HSV-1 replication as measured by extracellular viral titre (Fig. 6b-e and Extended Data Fig. 9d,e). Notably, mutations in VP22 (E77A and E257A) and in gD reduced the extracellular HSV-1 titre by ~10–50-fold (Fig. 6b). The gB-D66A mutation severely impaired HSV-1 lytic replication to the extent that amplification of the recombinant HSV-1 was unsuccessful. Conversely, an HSV-1 revertant containing gB-A66D behaved similarly to wild-type HSV-1, excluding the contribution of undesired mutations (Extended Data Fig. 9f). By contrast, the mutations abolishing the three ADP-ribosylations or polyADP-ribosylations of VP22 had no detectable effect on HSV-1 lytic replication (Fig. 6f). These results collectively support a distinct role of phosphoribosylation in HSV-1 lytic replication.

Considering the effect of phosphoribosylation-resistant mutations in VP22, gB and gD on HSV-1 replication, we analysed HSV-1 virions for viral structural proteins by immunoblotting. As shown in Fig. 6g, E77A and E257A had no effect on the virion incorporation of VP22 and VP16 but reduced that of gD, gH and UL37 while increasing the more slowly migrating (presumably more glycosylated) species of gB, despite all viral proteins being equally expressed in HSV-1-infected cells. In cells infected with HSV-1 containing gD-D297A, gD expression was greatly reduced while gB migrated much faster than that produced from the HSV-1 wild type, probably reflecting its lack of proper glycosylation (Fig. 6g). In HSV-1 virions containing gD-D297A, gD-D297A and UL37 were greatly reduced compared to wild-type HSV-1, whereas virion incorporation of gH and VP22, and to a lesser extent, that of gB and VP16, clearly increased (Fig. 6h). Importantly,

both gD-D297A and gH-D794A altered the expression of glycoproteins and tegument proteins in HSV-1-infected cells, which do not correlate with their virion incorporation. Though gH-D794A had the same effect on gB expression in HSV-1-infected cells as gD-D297A, it demonstrated a distinct impact on the virion incorporation of gH and VP22 (Fig. 6f). Thus, phosphoribosylation of VP22 and these glycoproteins affects the processing (for example, glycosylation) and virion incorporation of glycoproteins.

Phosphoribose on structural proteins enhances HSV-1 entry

Glycoproteins, including gB, gD, gH and gL, constitute a multicomponent machinery that mediates HSV-1 entry[28,29]. Along with the observation that mutations in VP22 affect the virion incorporation of multiple glycoproteins, phosphoribosylation of three out of four key entry glycoproteins prompted us to examine its role in HSV-1 entry. We first generated chimeric HSV-1 carrying both wild-type and phosphoribosylation-resistant mutants of gB, gD and gH as described in Fig. 5c for the entry assay. To do so, 293T cells over-expressing phosphoribosylation-resistant mutants of gB, gD and gH were infected with wild-type HSV-1 to produce chimeric HSV-1 (Fig. 7a). When HSV-1 entry was analysed by intracellular viral genomes, we found that phosphoribosylation-resistant gD and gB reduced HSV-1 entry by ~85% and ~60%, respectively, whereas phosphoribosylation-resistant gH had no significant effect (Fig. 7b). Given the reduced virion incorporation of gD-D297A and gB-D66A (Fig. 5e,f), the effect of these phosphoribosylation-resistant mutants on HSV-1 entry is probably underestimated. Next, we used recombinant HSV-1 carrying phosphoribosylation-resistant mutants of gD and gH for the entry assay, although the insufficiency of HSV-1 containing gB-D66A precluded a quantitative analysis of its effect on HSV-1 entry. Indeed, recombinant HSV-1 containing gD-D297A demonstrated a 50–75% reduction in entry, whereas chimeric HSV-1 containing the gH-D794A mutant showed no significant deficiency compared to wild-type HSV-1 (Fig. 7c,d). Similarly, recombinant HSV-1 carrying phosphoribosylation-resistant mutations—that is, E77A or E257A—in VP22 also demonstrated reduced HSV-1 entry compared to wild-type HSV-1 (Fig. 7e). Finally, HSV-1 virions produced from NAMPT-KO HeLa cells demonstrated ~2.5-fold more entry than those produced from wild-type HeLa cells, and the re-expression of NAMPT in NAMPT-KO HepG2 cells abolished the increase in HSV-1 entry (Fig. 7f). These results collectively show that phosphoribosylation of gB and gD is required for efficient HSV-1 entry.

To further examine the role of NAMPT-mediated antiviral restriction on HSV-1 entry, we treated HSV-1 virions produced from NAMPT-KO HepG2 cells with either NAMPT or the NAMPT-H247E mutant. We examined HSV-1 entry, quantified phosphoribose and analysed glycoproteins by two-dimensional gel electrophoresis (Fig. 7g). This analysis showed that wild-type NAMPT and TARG1, but not NAMPT-H247E, reduced HSV-1 entry by ~55% (Fig. 7h). Interestingly, the NAMPT-mediated inhibition requires ATP, which is consistent with the ATP-dependent activation of NAMPT (Extended Data Fig. 10a). Consistent with this result, NAMPT, but not the NAMPT-H247E mutant, released a significant amount of phosphoribose from HSV-1 virions, as quantified by LC–MS (Fig. 7i). Furthermore, NAMPT and TARG1 also increased the relative amount of the more positively charged species of gD and gB in HSV-1 virions, as shown by two-dimensional gel electrophoresis,

but the NAMPT-H247E mutant had little or no effect, supporting the phosphoribosylase activity of NAMPT toward HSV-1 glycoproteins (Fig. 7j and Extended Data Fig. 10b). When NAM was added to assess the phosphoribosyltransferase activity of NAMPT, we found that NAMPT extracted phosphoribose but failed to synthesize NMN (Extended Data Fig. 10c). As expected, NAMPT converted NAM into NMN when exogenous PRPP was added. Thus, this result also suggests that the released phosphoribose was not used to synthesize NMN or PRPP in the phosphoribosylase reaction. These results characterized a number of phosphoribosylation-resistant mutations of tegument and glycosylated proteins in HSV-1 virion assembly and entry (Extended Data Fig. 10d), demonstrating pivotal roles of protein phosphoribosylation in HSV-1 infection.

Discussion

Viral infections represent major challenges to public health, as evidenced by the recent COVID-19 pandemic, and the development of innovative therapeutic strategies will require a better understanding of host antiviral defence. Known as a metabolic phosphoribosyltransferase in salvage NAD^+ synthesis, NAMPT inhibits a handful of enveloped viruses, including West Nile virus, Venezuelan equine encephalitis virus and HIV-1 (refs. 30,31). In this study, we show that NAMPT acts as a phosphoribosylase toward several viral structural proteins to restrict HSV-1 lytic replication, ascribing unprecedented enzymatic activity to a key metabolic enzyme. Previously, antiviral metabolic enzymes were reported to impede viral replication processes by modifying key metabolites, such as SAMHD1 for HIV and viperin for various RNA viruses[4,5], or by evading the host immune response as observed with glutamine amidotransferases[32,33]. NAMPT recycles NAM to generate NAD^+, which is crucial for further downstream biological processes such as DNA damage response, epigenetic regulation and gene expression, all of which contribute to an efficient productive infection of HSV-1. By contrast, NAMPT de-phosphoribosylates viral, and probably cellular, proteins to hinder the assembly and subsequent infection of HSV-1 virions, thus qualifying as a ‘moonlighting’ enzyme[34]. When the enzyme activities of NAMPT were examined by V_{max} and K_{cat}, the protein phosphoribosylase activity is close to, although lower than, the phosphoribosyltransferase activity, suggesting that NAMPT primarily functions in NMN synthesis if NAM is available. When NAM is lower or not available within a subcellular locality such as the TGN, in which HSV-1 tegumentation occurs, NAMPT may act as a phosphoribosylase toward viral structural proteins. Indeed, NAMPT demonstrates antiviral activity against HSV-1 in HeLa and HepG2 cells in that NAM levels were reduced by HSV-1 infection compared to that of mock-infected cells, a scenario that favours the phosphoribosylase activity of NAMPT. This is supported by the observation that the expression of NAMPT-H247E reduced the percentage of the total phosphoribosylated peptides by >91% while increasing that of phosphoribosylated viral peptides by ~onefold. A notable limitation of the protein phosphoribosylase activity of NAMPT is that it was determined with purified HSV-1 virions that represent mixed protein substrates, which may complicate the interpretation of NAMPT’s phosphoribosylase activity. Additionally, we are unable to quantify phosphoribosylated peptides using NAMPT-treated HSV-1 proteins, largely because of the limited detection of phosphoribosylated peptides. Future phosphoribosylase

experiments involving a homogenously phosphoribosylated substrate and an efficient enrichment protocol will be necessary to better define the enzymatic activity of NAMPT. Intriguingly, ADP-ribose metabolic enzymes such as TARG1 were originally discovered to act on proteins as a terminal glycohydrolase and recently found to have demonstrated similar activity towards RNA and DNA[35,36], mirroring the two activities of NAMPT toward proteins and NAM. The phosphoribosyltransferase and phosphoribosylase activities of NAMPT toward small molecules and proteins, respectively, may also have a role in other microbial infections and human diseases[8,16]. This calls for further investigation into the dynamic regulation of these two activities.

NAMPT catalyses the synthesis of NAD^+ by salvaging NAM, which is the byproduct of predominant NAD^+-consuming enzymes such as polyADP-ribose polymerases, SIRTs and SARM1. Considering the essential roles of NAD^+ in diverse biological processes, it is surprising that NAMPT deficiency increased HSV-1 lytic replication. Indeed, the addition of NR to the medium effectively restores intracellular NAD^+ concentration and further boosts HSV-1 replication in NAMPT-KO or NAMPT-depleted cells, suggesting that the antiviral activity of NAMPT is probably underestimated. Previous studies have shown that global deletion of NAMPT is lethal in mice, largely owing to deficits in neurodevelopment[37,38]. In the global inducible KO mouse strain used in this study, significant depletion of NAMPT was observed only in the liver and spleen and not in the heart, lung and kidney upon induction with tamoxifen. This may explain the lack of apparent abnormalities in these mice. NAMPT deletion in the liver reduced hepatic abundance of NAD^+ by ~50%, which was restored by exogenous NR through intraperitoneal injection. This scenario resembles NAMPT-depleted cells cultured with the medium containing regular FBS. Consistently, NR administration to NAMPT-KO mice also increased HSV-1 replication in the NAMPT-depleted liver. Given the short duration of HSV-1 lytic replication in mice, we profiled innate immune gene expression in cells and the liver with NAMPT depletion and found that NAMPT depletion slightly increased the expression of some immune genes, possibly because of elevated HSV-1 lytic replication. These results support the notion that the loss of NAMPT does not grossly impair innate immune defence against HSV-1 in the *Nampt*$^{flox/flox}$:*cre* mice, and NR supplementation further increases HSV-1 lytic replication in NAMPT-depleted cells.

In metazoans, phosphoribose on proteins was previously identified through in-depth analysis of phosphoproteomic datasets, but no related functions have yet been described[25]. SdeA, an effector protein secreted by *Legionella pneumophila*, catalyses the phosphoribosylation of ubiquitin that is subsequently transferred to a target protein, thereby impairing cellular ubiquitination processes[39]. Considered relics of ADP-ribosylation and polyADP-ribosylation, phosphoribose moieties are probably derived from ADP-ribose and polyADP-ribose through enzymes like NUDT16, which has demonstrated the ability to convert ADP-ribose and polyADP-ribose into phosphoribose in assembled reactions[14]. However, whether NAMPT can directly add phosphoribosyl moieties to proteins remains unknown. These questions require further investigation.

Among the three ADP-ribosylation sites and four phosphoribosylation sites identified within VP22, none of these sites contain both phosphoribosyl and ADP-ribosyl

moieties. Conceivably, this may stem from the limited detection of ADP-ribosylated and phosphoribosylated peptides. Nevertheless, this finding supports the notion that ADP-ribosyl and phosphoribosyl units represent distinct biochemical and functional entities of VP22. Indeed, mutational analyses further showed that two phosphoribosylation-resistant mutations, but none of the three ADP-ribosylation-resistant mutations, significantly reduced HSV-1 lytic replication. Furthermore, the phosphoribosylation of multiple glycoproteins and the VP22 tegument protein functionally converge to impinge on virion assembly and infectivity, signifying the pivotal roles of phosphoribosylation in late stages of HSV-1 lytic replication. This conclusion is substantiated by electron microscopy analysis showing that NAMPT acts in the TGN during HSV-1 tegumentation, a fundamental process shared by all herpesviruses and probably other large enveloped RNA viruses. Notably, the biology of herpesviral tegumentation and protein phosphoribosylation is poorly understood. Herpesvirus infection, therefore, provides an excellent model system to address key questions concerning protein phosphoribosylation in assembly and egress in HSV-1 infection in particular and the fundamental biological processes in metazoans in general.

Although our results support the hepatocyte-intrinsic antiviral activity of NAMPT in mice, we could not exclude the possible roles of NAMPT in immune cells that control HSV-1 infection. When the phosphoribosylase activity of NAMPT was determined, purified HSV-1 virions were used to obtain V_{max} and K_{cat} by quantifying released phosphoribose but not phosphoribosylated peptides. Phosphoribosylation-resistant mutations can prevent ADP-ribosylation and other related modifications. Phenotypes of these mutations may embody the overall biological consequence of those modifications.

Methods

Cell culture

HEK293T, HepG2, HeLa, Vero and human foreskin fibroblast cells were purchased from ATCC, and mouse embryonic fibroblasts were isolated from the embryo of a *Nampt*^{tm1Oleo}:CreERT2 mouse. All cell lines were cultured in DMEM (HyClone) supplemented with 10% heat-inactivated FBS (Gibco) and 1% penicillin–streptomycin (Corning) and maintained in a humidified incubator with 5% CO_2 at 37 °C. Control (sgCTL) and NAMPT-KO (sgNAMPT) cells were generated using a CRISPR–Cas9 system. In brief, sgNAMPT or sgCTL constructs (pL-CRISPR-EFS-PAC, Addgene) and lentiviral packaging plasmids pMD2.g and psPAX (primers and constructs are described in Supplementary Table 10) were transfected into 293T cells for lentivirus production. At 48 h post transfection, the supernatant containing sgNAMPT or sgCTL lentivirus was collected, filtered through a 0.22 μm membrane and added to 293T, HepG2 and HeLa cells for spinfection with 8 μg ml^{-1} polybrene at 1,000*g* for 45 min. At 48 h post infection, puromycin was used to select cells at a final concentration of 2 μg ml^{-1}. To select a single colony, pooled puromycin-resistant cells were diluted into 96 well plates to achieve a single cell per well. Each colony was expanded and further validated by western blot and genomic sequencing. The sgNAMPT cells were maintained in complete DMEM supplemented with 0.1 mM NR.

To generate the reconstituted cell lines, sgNAMPT cells were spinfected with lentiviruses carrying NAMPT, including NAMPT–FLAG, NAMPT–V5, NAMPT–HA, NAMPT-H247E–

FLAG and NAMPT-D219A–FLAG. The expression of wild-type NAMPT and mutants was validated by western blot with antibodies to NAMPT or the corresponding epitope.

Viral infection and titration

To perform HSV-1 infection and determine the virus growth curve, NAMPT knockdown or KO and control cells were infected with HSV-1 at a multiplicity of infection of 0.1 in FBS-free DMEM medium for 2 h. Fresh DMEM medium containing 10% dialyzed FBS, supplemented with 0.1 mM NR, was used to replace the infection medium. The medium and cells were collected separately at 12, 24, 36, 48 and 72 h post infection for plaque assay to determine viral titre.

The HSV-1 titre was determined by plaque assay on a Vero monolayer. In brief, a tenfold serial-diluted virus-containing medium (FBS-free DMEM) was added to Vero cells. After 2 h of incubation in 5% CO_2 at 37 °C, DMEM containing 10% FBS and 1% methylcellulose (Sigma-Aldrich) was overlaid to infected Vero cells for plaque formation. At 3 days post infection, Vero monolayers were stained with 1% crystal violet for plaque counting.

Mice

Nampt^{tm1Oleo} mice (Jax stock *Nampt*^{tm1Oleo}/ImaiJ; strain no. 034242) were gifted from Prof. Shin-ichiro Imai at the Washington University School of Medicine[40]. *Nampt*^{tm1Oleo} mice were crossed with CreERT2 mice (Jax stock B6;129-*Gt(ROSA)26Sor*$^{tm1(cre/ERT2)Tyj}$/J, Jax strain no. 008463) from Jackson Laboratories. Primers used in genotyping are listed in Supplementary Table 10. The PCR conditions are as follows: 20 s at 95 °C, 30 s at 55 °C and 30 s at 72 °C for 30 cycles. To generate *Nampt*$^{-/-}$ mice, *Nampt*^{tm1Oleo}:CreERT2 mice were injected intraperitoneally with tamoxifen in Kolliphor EL (75 mg kg^{-1}) for 5 days. To restore NAD^+, 400 mg kg^{-1} of NR was supplemented daily by intraperitoneal injection[41]. Age-matched (12–14-week-old) and sex-matched mice were used for all experiments unless specified otherwise. All animal experiments were performed in accordance with the Guide for the Care and Use of Laboratory Animals of the National Institutes of Health. The animal protocol was approved by the Institutional Animal Care and Use Committee of the University of Southern California.

For HSV-1 infection, age-matched and sex-matched mice were challenged with HSV-1 (5×10^7 PFU) in 100 µl of PBS by intravenous injection 5 days after tamoxifen treatment. Mouse survival was monitored daily for 20 days. To titrate viral replication and analyse immune responses, infected mice were killed 3 days post infection and the tissues and organs were collected. One piece of the liver was fixed in 4% paraformaldehyde for histology analysis, and the remaining liver and spleen tissues were homogenized with Zirconia/Silica Beads in a beats beater (BioSpec Products) for immunoblotting, DNA and RNA extraction and virus titration. HSV-1 titre was determined by plaque assay, cytokine transcripts (after reverse transcription) and viral DNA were measured by real-time quantitative PCR with reverse transcription (RT–qPCR). To evaluate the role of NR in HSV-1 infection in mice, a slightly lower dose of HSV-1 (2×10^7 PFU) was used in 100 µl of PBS for intravenous injection 5 days after tamoxifen treatment. Mouse survival was monitored daily for up to 20 days, and

tissues were collected for metabolite analysis, viral titration, immunoblotting, and DNA and RNA extraction when the mice were killed.

NAMPT protein expression and purification

Human NAMPT (encoding residues 1-491) cDNAs, including wild-type, H247E and D219A, were cloned into the pGEX-4T-1 bacterial expression vector, with a TEV protease recognition site inserted downstream of the GST open reading frame. The NAMPT constructs were transformed into BL21 *Escherichia coli* competent cells. After induction at 20 °C overnight, the bacterial pellet was lysed, sonicated and centrifuged at 12,000 r.p.m. (J-LITE JLA-16.250, Beckman) for 20 min at 4 °C. The cleared lysate was mixed with Glutathione Sepharose 4B (Sigma-Aldrich, GE17-0756-01) and incubated at 4 °C for 2 h with constant rotation. Glutathione beads were washed three times with 20 mM Tris pH 7.5 and 0.1% Triton X-100 and proteins were eluted with 10 mM reduced glutathione in 50 mM Tris pH 8.0. Purified protein was analysed and quantified by SDS–PAGE and Coomassie staining and stored in 10% glycerol at −80 °C for in vitro reactions.

HSV-1 DNA extraction

To extract the viral DNA in the supernatant, virions were pelleted by high-speed ultracentrifugation at 80,000*g* for 1 h at 4 °C. Viral DNA and cellular DNA were extracted as previously reported with minor modifications[42]. In brief, the tissue, cell and virion samples were lysed in NK Lysis Buffer (50 mM Tris, 50 mM EDTA, 1% SDS, pH 8) with proteinase K and incubated at 55 °C overnight. RNase A was used to remove RNA. Samples were cooled on ice before the addition of pre-chilled 7.5 M ammonium acetate to precipitate proteins. After vortexing, the samples were centrifuged at 4,000*g* for 10 min and the supernatant was carefully transferred into a new tube. To pellet down genomic DNA, 60% (v/v) isopropanol was added to the tube, followed by inverting 20 times and centrifugation at 15,000*g* for 10 min. The DNA pellet was washed with freshly prepared 70% ethanol. After air drying for 10–30 min, 1× TE buffer was added to fully dissolve the DNA pellet.

RNA extraction and real-time RT–qPCR

Cellular total RNA was extracted using TRIzol reagent (Invitrogen) per the manufacturer's instructions. Mouse tissue RNA was extracted using the RNeasy Mini Kit (QIAGEN, 74106) following the manufacturer's instructions. A total of 1 μg RNA, treated with DNase I, was used as a template to synthesize cDNA with M-MLV reverse transcriptase (Promega, M1701). Each real-time RT–qPCR reaction was assembled with a cDNA template, corresponding primer set (Supplementary Table 10) and SYBR master mix (Applied Biosystems). Cycle conditions were as follows: 95 °C for 10 min and 95 °C for 15 s followed by 55 °C for 1 min (40 cycles). Relative mRNA expression for each target gene was calculated by the $2^{-\Delta\Delta Ct}$ method, normalized to the *Actb* for mouse or *ACTB* for human.

Immunohistochemical, immunofluorescence analysis and H&E staining

To visualize the expression of NAMPT and viral proteins, extracted liver tissues were first fixed in 4% paraformaldehyde solution (Sigma-Aldrich) for 24 h at 4 °C. After dehydration in 70%, 80%, 95% and 100% ethanol (v/v in water) and xylene, tissues were embedded in paraffin and sliced into 4-μm sections. For immunohistochemistry staining, the sections were deparaffinated, rehydrated and oxidized. Processed sections were blocked with 10% goat serum for 1 h and incubated with the primary antibodies at 4 °C overnight. After washing with PBST, sections were probed with horseradish peroxidase-linked secondary antibody (A120-101P, Bethyl Laboratories) for 40 min at 37 °C, reacted with diaminobenzidine (Leica) and counterstained with Mayer hematoxylin (Leica).

To perform H&E staining, deparaffinated sections were incubated with hematoxylin for 30 s and rinsed with de-ionized water, followed by eosin staining for 30 s before dehydration and mounting. Each section was evaluated and captured under an inverted confocal microscope (Nikon Eclipse Ti2) equipped with a ×10–40 objective.

To determine the incorporation of NAMPT into HSV-1 virion particles, sgNAMPT HeLa cells stably reconstituted with NAMPT–HA were grown on poly-l-lysine-coated coverslips and infected with HSV-1. The cells were fixed with 4% paraformaldehyde and permeabilized with 0.1% Triton X-100. After blocking with 5% BSA in PBS, samples were incubated with primary antibodies at 4 °C overnight, followed by incubation with dye-conjugated secondary antibodies for 1 h at room temperature (21–23 °C). Imaging was performed using a Nikon Eclipse Ti microscope with NIS-Elements AR imaging software.

Sucrose gradient centrifugation

At 48 h post HSV-1 infection, the HSV-1-containing medium was collected, centrifuged at 4,000 r.p.m. for 10 min and filtered through a 0.22-μm membrane. Virions were further pelleted by centrifugation at 80,000*g* (Beckman TYPE45) for 60 min at 4 °C and resuspended in TNE buffer (0.01 M Tris-HCl, 0.5 M NaCl, 1 mM EDTA, pH 7.5)[43,44]. Resuspended virions were loaded onto the top of the 15–55% (w/v) sucrose gradient and centrifuged at 80,000*g* for 60 min at 4 °C in a Beckman SW41 rotor. A total of 12 fractions, 1 ml sucrose solution for each, were collected and analysed by SDS–PAGE and immunoblotting analysis with antibodies against HSV-1 antigens. Virions were observed as milky bands identified by scattered light. The virion band was further pelleted and resuspended in PBS or in vitro assay buffer (see in vitro phosphoribosylase activity assay) for further biochemical and microscopic analyses. Extraction of NAMPT exosomes (FLAG–NAMPT) followed published protocols[17,45] and was validated by immunoblotting with antibodies against CD81 (1:1,000, Santa Cruz, sc-166029), Alix (1:1,000, Santa Cruz, sc-53540), CD63 (1:500, BD Pharmingen, 556019) and Calnexin (1:1,000, Cell Signaling, C5C9).

Co-sedimentation assay and proteinase K digestion

Proteinase K (final concentration, 50 μg ml^{-1}) or Triton X-100 (final concentration, 1%) was added to the purified virion suspension and incubated for 5 min at 55 °C. The proteinase activity was terminated by adding 5 mM phenylmethylsulfonyl fluoride for 10 min at room

temperature. Alternatively, HSV-1 virions treated with NP-40 buffer (1%) were incubated with recombinant NAMPT protein and centrifuged through a sucrose gradient[46]. Nuclear capsids were collected and analysed by immunoblotting with antibodies against HSV-1 gB, tegument UL37 and major capsid protein UL19.

Immunogold staining and transmission electron microscopy

For transmission electron microscopy, HSV-1 virions were purified from sgNAMPT HeLa cells reconstituted with HA–NAMPT. Purified viral particles were pretreated with 2% Triton X-100 and 2% glutaraldehyde for 30 min. Viral particles were adsorbed on formvar-carbon-coated nickel grids for 30 min. To prepare cell sections for transmission electron microscopy, cells were fixed with 4% paraformaldehyde and 0.05% glutaraldehyde in PIPES buffer for 1 h on ice. Cells were dehydrated, sectioned and placed on grids.

For immunogold labelling, the samples were incubated in blocking buffer (PBS, 1% BSA and 1% Tween-20) for 1 h followed by the incubation with primary antibodies (anti-HA for NAMPT, rabbit polyclonal HA antibody, BioLegend, cat no. 901501, RRID: AB_2565006, dilution: 1:100; anti-UL19, mouse monoclonal [3B6] to HSV1 + HSV2 UL19 major capsid protein, Abcam, cat no. ab6508, RRID: AB_305530, dilution 1:100; anti-TGN46, Sigma-Aldrich, cat no. ABT95, dilution 1:100) at 4 °C overnight and gold-conjugated secondary antibodies (1:500) at room temperature for 1 h. After being rinsed with fresh PBS containing 1% Tween-20, grids were stained with 1% uranyl acetate (10 min at room temperature) followed by 0.25% lead citrate (2 min at room temperature) and air dried. All electron microscopy analyses were carried out on a JEOL 2100 transmission electron microscope operated at 50 keV.

Protein identification for APEX-mediated biotinylation by mass spectrometry

HSV-1-infected HeLa cells were collected and lysed in RIPA buffer, and biotinylated proteins were precipitated with streptavidin beads. After extensive washing with lysis buffer, the streptavidin beads were further washed three times with 25 mM ammonium bicarbonate. On-bead digestion was performed by reducing the proteins with 10 mM dithiothreitol (DTT) at 37 °C for 15 min, followed by alkylation with 10 mM IAA in the dark at room temperature for 15 min. The proteins were then digested overnight at 37 °C with trypsin (G-Biosciences) at an enzyme-to-substrate ratio of 1:100 (w/w). Digested peptides were further desalted using a C18 tip (P200 Toptip, PolyLC) following the manufacturer's instructions and then dried in a rotary evaporator. Peptides were reconstituted in 0.1% formic acid (FA) for nano LC–tandem mass spectrometry (LC–MS/MS) analysis on a Q-Exactive Plus hybrid quadrupole-Orbitrap mass spectrometer (ThermoFisher Scientific) equipped with a Dionex UltiMate 3000 HPLC system (ThermoFisher Scientific). Peptides were separated on the heated EASY-Spray analytical column (C18, 2 μm, 100 Å, 75 μm × 25 cm, ThermoFisher Scientific) with a flow rate of 0.3 μl min^{-1} for a total duration of 75 min and then ionized at 2.0 kV in the positive ion mode. The gradient was composed of 3–38% buffer B (60 min) followed by the wash step at 98% B (15 min); solvent A: 0.1% FA; solvent B: 80% ACN and 0.1% FA. MS1 scans for data-dependent acquisition were acquired at the resolution of 70,000 from 350 to 1800 m/z, automatic gain control (AGC) target of 1×10^6 and a maximum injection time of 100 ms. The ten most abundant ions in the MS1 scans

were selected for fragmentation via higher-energy collisional dissociation with a normalized collision energy of 28, and MS2 scans were acquired at a resolution of 17,500, AGC target 5×10^4, maximum injection time of 120 ms and normalized collision energy of 28. Dynamic exclusion was set to 30 s and ions with charges of +1, +7 and >+7 were excluded. MS2 fragmentation spectra were searched with Proteome Discoverer Sequest HT (v.2.4, Thermo Scientific) against in silico tryptic digested combined Uniprot Human herpesvirus 1 (HHV-1) database (UP000009294, downloaded on 11 December 2019) concatenated with the Uniprot reviewed human database (UP000005640, downloaded on 24 October 2021). The maximum missed cleavages were set to two. Dynamic modifications were set to oxidation on methionine (M, +15.995 Da). Carbamidomethylation on cysteine (C, +57.021 Da) was set as a fixed modification. The maximum parental mass error was set to 10 ppm, and the MS2 mass tolerance was set to 0.02 Da. The false discovery threshold was set strictly to 0.01 using the Percolator Node validated by *q*-value. The frequency of peptide spectrum matches was used as a proxy of protein abundance in the samples[47].

Proteomics analysis for phosphoribosylated peptides

For proteomics of HSV-1 infected cells, cells were lysed and digested in an S-Trap micro spin column (Protifi) according to the manufacturer's instructions. After elution and drying, peptides were suspended in LC–MS-grade water containing 0.2% FA and 2% acetonitrile for further LC–MS/MS analysis. For the identification of phosphoribosylated peptides, cells were lysed in 8 M urea in 100 mM Tris-HCl, pH 7 and sonicated on ice for 10 min (30 s pulse with 30 s rest in between). Lysates were centrifuged at 16,000*g* for 5 min and protein concentration was determined using the BCA protein assay. Then, 300 μg of the sample was reduced with 5 mM DTT in a 37 °C water bath for 10 min and alkylated with 10 mM iodoacetamide for 30 min in the dark at room temperature. After alkylation, the samples were diluted to 1 M urea with 100 mM Tris-HCl, pH 7. To digest the protein, trypsin (G-Biosciences) was first added at a 1:100 enzyme-to-substrate ratio (w/w) and reactions were incubated overnight at 37 °C. Subsequently, sequential digestion with chymotrypsin (G-Biosciences) was performed at a 1:20 enzyme-to-substrate ratio (w/w) at room temperature for 6 h. Peptides were desalted in a C18 tip (P200 Toptip, PolyLC) following the manufacturer's instructions and then dried in a rotary evaporator. The immobilized metal affinity chromatography phosphoenrichment method was modified based on a previously described method[48]. In brief, 100 μg of peptides were reconstituted in 150 μl of binding buffer (0.1% FA and 40% acetonitrile) and incubated with 50 μl of pre-equilibrated PHOS-Select beads (Sigma-Aldrich) at room temperature for 1 h. The beads were then transferred to pre-equilibrated C18 TopTips, washed twice with 200 μl of binding buffer, acidified with 200 μl of 1% FA, eluted onto the low layer of C18 TopTips with 200 μl of 0.5 M K_2HPO_4, pH 7. The C18 TopTips were washed with 0.1% FA and desalting buffer A (5% acetonitrile, 0.1% TFA) and then eluted with desalting buffer B (80% acetonitrile, 0.1% TFA). Eluted peptides were dried and reconstituted in 0.2% FA and 2% acetonitrile for LC–MS/MS analysis.

Purified HSV-1 virion and GST–VP22 on glutathione agarose were subjected to digestion, with or without immobilized metal affinity chromatography enrichment. After in vitro

reaction, agarose-bound GST–VP22 was washed with 20 mM ammonium bicarbonate (pH 7.8). These protein samples were processed as described above.

Phosphoribosylated peptides were analysed on an EASY-nLC 1200 coupled to an Orbitrap Eclipse Tribrid mass spectrometer (ThermoFisher Scientific). Peptides were separated on an Aurora UHPLC Column (25 cm × 75 μm, 1.6 μm C18, AUR2-25075C18A, Ion Optics) with a flow rate of 0.35 μl min^{-1} for a total duration of 135 min and ionized at 1.6 kV in the positive ion mode. When whole cell lysates were analysed, an extended programme with a duration of 270 min was used to increase the depth of peptide identification. The gradient was composed of 6% solvent B (7.5 min), 6–25% B (82.5 min), 25–40% B (30 min) and 40–98% B (15 min); solvent A: 0.1% FA in water; solvent B: 80% ACN and 0.1% FA. MS1 scans were acquired in the Orbitrap at the resolution of 120,000 from 350 to 2,000 m/z, AGC of 1×10^6, and a maximum injection time of 50 ms. MS2 scans were obtained in the ion trap using fast scan rate on precursors with two to seven charge states and quadrupole isolation mode (isolation window, 0.7 m/z) with a higher-energy collisional dissociation (30%) activation type. Dynamic exclusion was set to 30 s. The temperature of the ion transfer tube was 300 °C and the S-lens RF level was set to 30.

MS2 fragmentation spectra were searched with both Sequest HT and MS Amanda 2.0 search engines within the Proteome Discoverer (v.2.5, Thermo Scientific). The search for HSV-1-infected cells was conducted using the combined Uniprot Human herpesvirus 1 (HHV-1) database (UP000009294, downloaded on 11 December 2019) and the Uniprot reviewed human database (UP000005640, downloaded on 24 October 2021). By contrast, the search for virions was performed against the HSV-1 proteome. The maximum missed cleavages were set to two. Dynamic modifications were set to oxidation on methionine (M, +15.995 Da), phosphoribosylation (D, E, R and K, +212.009 Da), deamidation (N and Q, +0.984 Da), protein N-terminal acetylation (+42.011 Da) and Met-loss (−131.040 Da). Carbamidomethylation on cysteine residues (C, +57.021 Da) was set as a fixed modification. The maximum parental mass error was set to 10 ppm, and the MS2 mass tolerance was set to 0.6 Da. The false discovery threshold was set strictly to 0.01 using the Percolator Node validated by q-value. The relative abundance of parental peptides was calculated by integration of the area under the curve of the MS1 peaks using the Minora LFQ node. The IMP-ptmRS node within the Proteome Discoverer was used to calculate PTM site probabilities. The mass spectrometry proteomics data was deposited to the ProteomeXchange Consortium via the PRIDE partner repository with the dataset identifier PXD050684.

Metabolite analysis by LC–MS

Mock-infected and HSV-1-infected cells (approximately 2×10^6) were first washed with PBS and ice-cold 150 mM ammonium acetate (NH_4AcO, pH 7.3). A total of 1 ml of cold 80% MeOH, pre-chilled at −80 °C, was added to cells to extract metabolites. After incubation at −80 °C for 20 min, cells were scraped off and pelleted at 4 °C for 10 min at 21,000g. The supernatant was transferred into new microfuge tubes and vacuum-dried at room temperature; then the pellet was resuspended in water for LC–MS analysis. Samples from in vitro assays were centrifuged to separate the protein and supernatant. The

supernatant was mixed with cold absolute MeOH to extract metabolites and vacuum-dried as described above. Resuspended samples were randomized and analysed on a Q-Exactive Plus hybrid quadrupole-Orbitrap mass spectrometer coupled with Vanquish UHPLC system (ThermoFisher Scientific) in polarity switching mode (+3.00 kV/−2.25 kV) with an m/z window ranging from 65 to 975. Mobile phase A was 5 mM NH_4AcO, pH 9.9, and mobile phase B was acetonitrile. Metabolites were separated on a Luna 3 μm NH2 100 NH2 100 A° (150 ×2.0 mm) column (Phenomenex), with a flow rate of 0.3 ml min^{-1}, gradient from 15% A to 95% A over 18 min, followed by an isocratic step for 9 min and re-equilibration for 7 min. Each metabolite was identified based on retention time and standard compound (Sigma-Aldrich) and quantified by peak area integration using TraceFinder v.4.1 (ThermoFisher Scientific).

Two-dimensional gel electrophoresis

Protein samples including whole cell lysates, purified virions and in vitro phosphoribosylase assay samples were resolved in 150 μl rehydration buffer (8 M urea, 50 mM DTT, 2% CHAPS, 0.5% IPG buffer and 0.002% bromophenol blue), followed by sonication for 20 s and centrifugation at 20,000*g* for 2 min. The supernatant was incubated with 6-11NL or 3-11NL IEF dry strips with the following running conditions: 20 V, 10 h; hold at 100 V, 1 h; 500 V, 1 h and 1,000 V, 1 h; gradient mode at 5,000 V for 4 h and hold at 5,000 V for 4 h. Before SDS–PAGE, strips were incubated with SDS-equilibration buffer (50 mM Tris-HCl (pH 8.8), 6 M urea, 30% glycerol, 2% SDS, 0.001% bromophenol blue) containing 10 mg ml^{-1} DTT for 15 min and that containing 25 mg ml^{-1} 2-iodoacetamide for 15 min. Strips were rinsed with SDS–PAGE buffer, resolved by SDS–PAGE and analysed by immunoblotting with the indicated primary antibodies. Primary antibodies used to probe GST or epitopes (V5, FLAG or HA) for HSV-1 proteins include mouse monoclonal GST antibody (Santa Cruz Biotechnology, cat. no. sc-138) diluted at 1:1,000; monoclonal FLAG M2 monoclonal antibody (Sigma-Aldrich, cat. no. F1804) diluted at 1:2,000; and rabbit polyclonal V5 antibody (Bethyl, cat. no. A190-120A, RRID: AB_67586) diluted at 1:1,000.

NAMPT phosphoribosyltransferase assay in salvage NAD^+ synthesis

NAMPT activity was assessed using CycLex NAMPT Colorimetric Assay Kit v.2 (MBL, CY-1251V2) per the manufacturer's instructions. In brief, purified wild-type NAMPT and NAMPT mutants, including NAMPT-H247E and NAMPT-D219A (tagged with either streptavidin-binding peptide or GST) were mixed with NAM, PRPP, ATP, diaphorase, ADH, NMN adenylyltransferase 1, WST-1 and ethanol in the Tris-HCl and $MgCl_2$ buffer. The mixture was incubated at 30 °C and the absorbance at 450 nm was determined to represent the enzymatic activity.

In vitro NAMPT protein phosphoribosylase assay

The in vitro protein phosphoribosylase assay was performed as previously described with modifications[49,50]. In brief, 5 μg of purified GST–VP22 or virions (~10 μg total viral proteins) was incubated with 1 μg of purified NAMPT or its mutants at 37 °C for 30 min in NAMPT reaction buffer (50 mM Tris-HCl (pH 7.5), 2 mM DTT, 10 mM $MgCl_2$ and 2 mM ATP). The reaction was stopped by adding rehydration buffer. VP22 was eluted and analysed by two-dimensional gel electrophoresis and immunoblotting.

To quantitatively determine phosphoribose released by NAMPT, up to 20 μg of purified HSV-1 virions and twofold dilutions were incubated with 1 μg of purified GST–NAMPT or the NAMPT-H247E mutant at 37 °C for 30 min in NAMPT reaction buffer. Before in vitro reaction, purified HSV-1 virions were extensively washed with in vitro reaction buffer to reduce the background of released phosphoribose. Reaction samples were centrifuged at 80,000*g* to pellet HSV-1 virions. The supernatant (80 μl) was mixed with 640 μl methanol (LC–MS/MS grade) to extract the metabolites that were then subjected to LC–MS analysis.

Co-immunoprecipitation

HEK293T cells were infected with HSV-1 or transfected with indicated plasmids for 36–48 h. Whole cell lysates were prepared with NP-40 lysis buffer (50 mM Tris-HCl, pH 7.4, 150 mM NaCl, 1% NP-40, 5 mM EDTA) supplemented with 20 mM β-glycerophosphate and 1 mM sodium orthovanadate. Samples were sonicated, centrifuged and pre-cleared with Sepharose 4B agarose beads (Sigma-Aldrich) for 1 h at 4 °C. Pre-cleared samples were incubated with ANTI-FLAG M2 Agarose Affinity Gel or Anti-V5 Agarose Affinity Gel (Bethyl Group) for 4 h at 4 °C. The agarose beads were washed extensively, and samples were eluted by boiling at 95 °C for 10 min. Precipitated proteins were analysed by SDS–PAGE and immunoblotting.

SDS–PAGE and immunoblotting

Tissues and cells were solubilized in lysis buffer (50 mM Tris-HCl, pH 7.4, 1 mM EDTA, 150 mM NaCl, 0.25% Na-deoxycholate, 1% NP-40, 0.10% SDS, 1% Triton X-100) on ice for 30 min and lysates were centrifuged at 12,000 r.p.m. at 4 °C for 20 min. Soluble fractions were denatured in loading buffer at 95 °C, separated by SDS–PAGE and subsequently transferred to nitrocellulose membranes. Membranes were blocked with 5% skim milk and probed with primary antibodies overnight at 4 °C, later incubated with secondary antibodies (IRDye800CW-conjugated or IRDye680RD-conjugated at 1:20,000 dilutions; LI-COR Biosciences) for 1 h before being exposed on the LI-COR Odyssey infrared imager. Images were processed using Image Studio v.5.0 and v.6.0 (LI-COR Biosciences); uncropped images are included in Source Data.

Primary antibodies (diluted 1:1,000) were used in this study: mouse monoclonal FLAG M2 antibody (Sigma-Aldrich, cat. no. F1804; RRID: AB_259529), mouse monoclonal V5 antibody (Abcam, cat. no. ab27671; RRID: AB_471093), mouse monoclonal β-actin antibody (Abcam, cat. no. ab8224; RRID: AB_449644), rabbit polyclonal UL37 antibody (Laboratory of P.F.), rabbit polyclonal NAMPT antibody (Bethyl Laboratories, cat. no. A300-372A, RRID: AB_2251232), 1:1,000; mouse monoclonal [3B6] to HSV1 + HSV2 UL19 major capsid protein (Abcam, cat. no. ab6508, RRID: AB_305530), mouse monoclonal HSV-1/2 gB antibody (Santa Cruz Biotechnology, cat. no. sc-56987; RRID: AB_629626), mouse monoclonal HSV-1 gD antibody (Santa Cruz Biotechnology, cat. no. sc-21719, RRID: AB_627720), rabbit polyclonal HA antibody (BioLegend, cat. no. 901501, RRID: AB_2565006), rabbit polyclonal V5 antibody (Bethyl, cat. no. A190-120A, RRID: AB_67586, 1:1,000), mouse monoclonal VP16 (Santa Cruz Biotechnology, cat. no. sc-7545), rabbit VP22 antibody (gifted by Dr. Chunfu Zheng, Fujian Medical University), rabbit gH antibody (gifted by Dr. Gary H. Cohen, University of Pennsylvania, 1:500) and

rabbit polyclonal anti-UL47 antibody (Laboratory of P.F., this study, 1:500). All rabbit antibodies against HSV-1 were used at 1:1,000 dilution if not specified.

Recombinant HSV-1

HSV-1 mutant viruses generated in this study were constructed by using an infectious clone of pBAC-HSV-1. Mutagenesis was created based on a markerless two-step Red recombination protocol (Extended Data Fig. 9a)[51]. In brief, linear PCR products, with a Kan cassette containing an *I-Sce*I homing endonuclease site and mutation site(s), were amplified using the pEPkan-S vector and primers with 60 bp homology to the region of interest. Purified PCR products were electroporated into GS1783 bacteria containing pBAC-HSV-1. The first lambda Red recombination incorporated the PCR product into the region of interest via homologous recombination. The second lambda Red recombination step was performed to remove the Kan^R-*I-Sce*I gene cassette, by using an *I-Sce*I homing endonuclease and the repeat sequence within the homologous arms of the inserted PCR products. Engineered pBAC-HSV-1 plasmids were extracted using the isopropanol precipitation method. The success of mutations was confirmed by PCR and sequencing. The primer sequences are listed in Supplementary Table 10.

To generate mutant HSV-1, approximately 1×10^6 Vero cells were transfected with 2 μg of extracted pBAC-HSV-1 DNA using Lipofectamine 3000 (Invitrogen). Viral plaques were observed at 48–72 h post transfection. Recombinant HSV-1 was subjected to two rounds of plaque purification, followed by three to four amplifications to produce sufficient viruses for biochemical and virological experiments.

HSV-1 entry assay

NAMPT-treated or recombinant HSV-1 virions were diluted in FBS-free DMEM and used to infect HeLa cells for up to 2 h. Infected cells were disassociated by trypsin digestion and washed extensively with PBS. Total genomic DNA was extracted, and the HSV-1 genome was quantified by real-time PCR using primers specific to HSV-1 genes, such as UL48 and UL37. To generate HSV-1 virions containing mutant viral proteins (such as VP22, gB, gD and gH), plasmids containing wild-type or mutant VP22, gD, gB and gH were first transfected into HEK293T cells. At 24 h post-transfection, cells were infected with wild-type HSV-1 at a multiplicity of infection of 0.1. HSV-1 progeny virions were collected and normalized by quantitative PCR for the viral genome. Equal amounts of the viruses were used for entry assay as described above.

Statistics and reproducibility

Data represent the mean of three independent experiments, and error bars denote s.d. unless specified otherwise. GraphPad Prism 9 v.4.0 and Prism 10 v.10.1.1 were used to analyse the mouse Kaplan–Meier survival curve, the log-rank test that was applied to the mouse survival data and the Michaelis–Menten modelling used to calculate V_{max} and K_{cat}. Statistical analysis was also performed with GraphPad Prism 10 for unpaired two-tailed *t*-tests and two-way ANOVA. A P value <0.05 was considered statistically significant. Unless otherwise specified, all data represent at least three independent experiments.

Extended Data

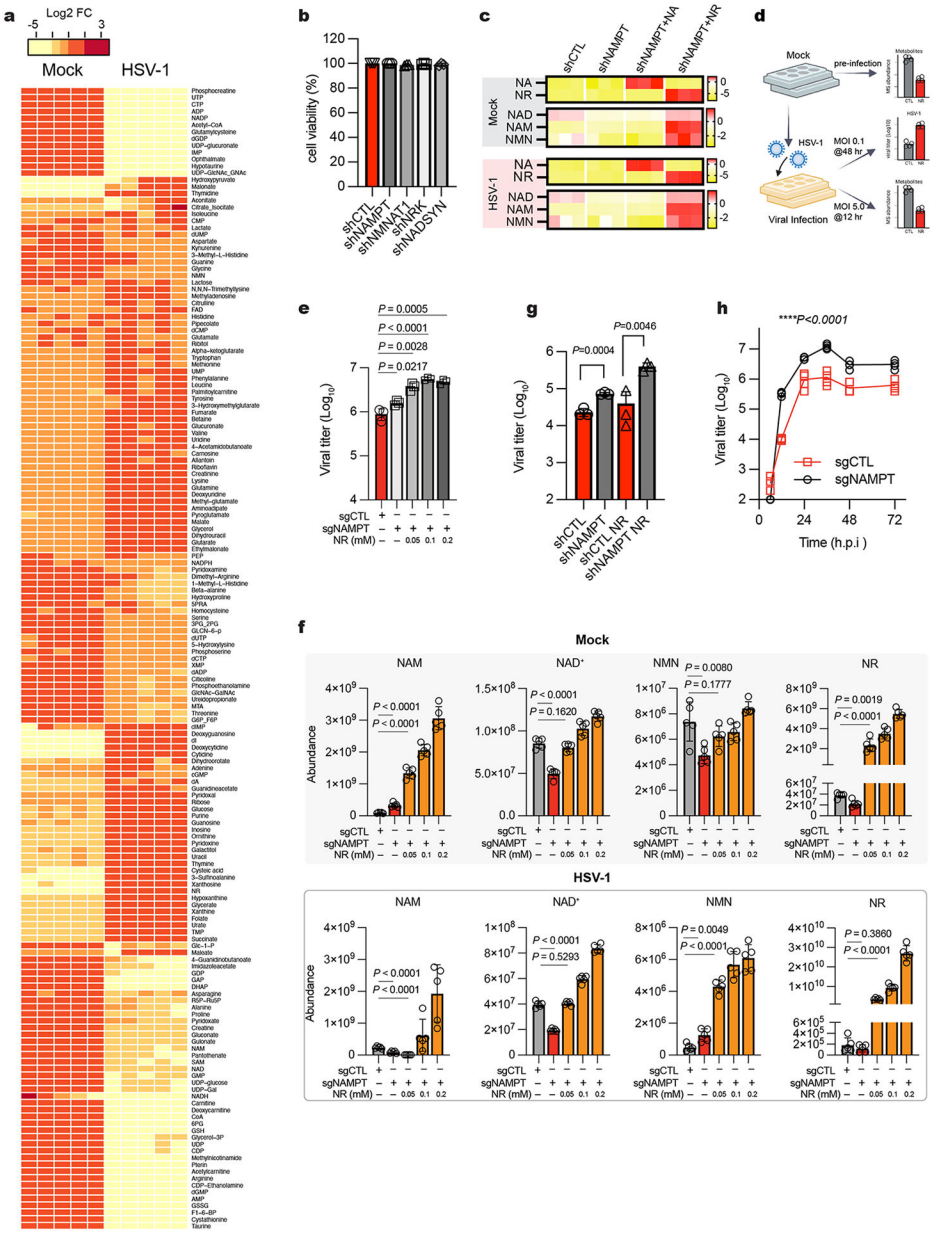

Extended Data Fig. 1 |. Metabolic alterations by HSV-1 during lytic replication.

a, Heatmap of metabolites profiled in mock- and HSV-1-infected HepG2 cells at 12 hours post-infection (h.p.i) (MOI = 5). **b**, Cell viability of 293 T cells depleted with NAMPT, NMNAT1, NRK, or NADSYN, n = 3. **c**, Quantification of NAD^+ and NMN in shNAMPT HeLa cells infected with HSV-1, supplemented with nicotinic acid (NA, 0.1 mM) or nicotinamide riboside (NR, 0.1 mM). **d-f**, Infection diagram (d) and HSV-1 titers (e, n = 3) in shCTL and shNAMPT HeLa cells with or without supplementation of NR, $P = 0.0217$ (no NR), $P = 0.0028$ (0.05 mM NR), $P < 0.0001$ (0.1 mM NR), $P = 0.0005$ (0.2 mM NR). Exogenous NR increases the abundance of the NAD^+-related metabolites in sgNAMPT HeLa cells in a dose-dependent manner, n = 5 (f). Diagram was created with Biorender.com.

g, HSV-1 titer in shCTL and shNAMPT HeLa cells without or with supplementation of nicotinamide riboside (NR, 0.1 mM) at 12 h.p.i. (MOI = 0.1), n = 3. **h**, Growth curve of HSV-1 is determined by intracellular virus in sgCTL and sgNAMPT HeLa cells, n = 4, P < 0.0001. Statistical significance was calculated using unpaired two-tailed *t*-tests, for d and f; two-way ANOVA for h. Data in b, d, f, h, and g are presented as mean values±SD. Graphics created with BioRender.com.

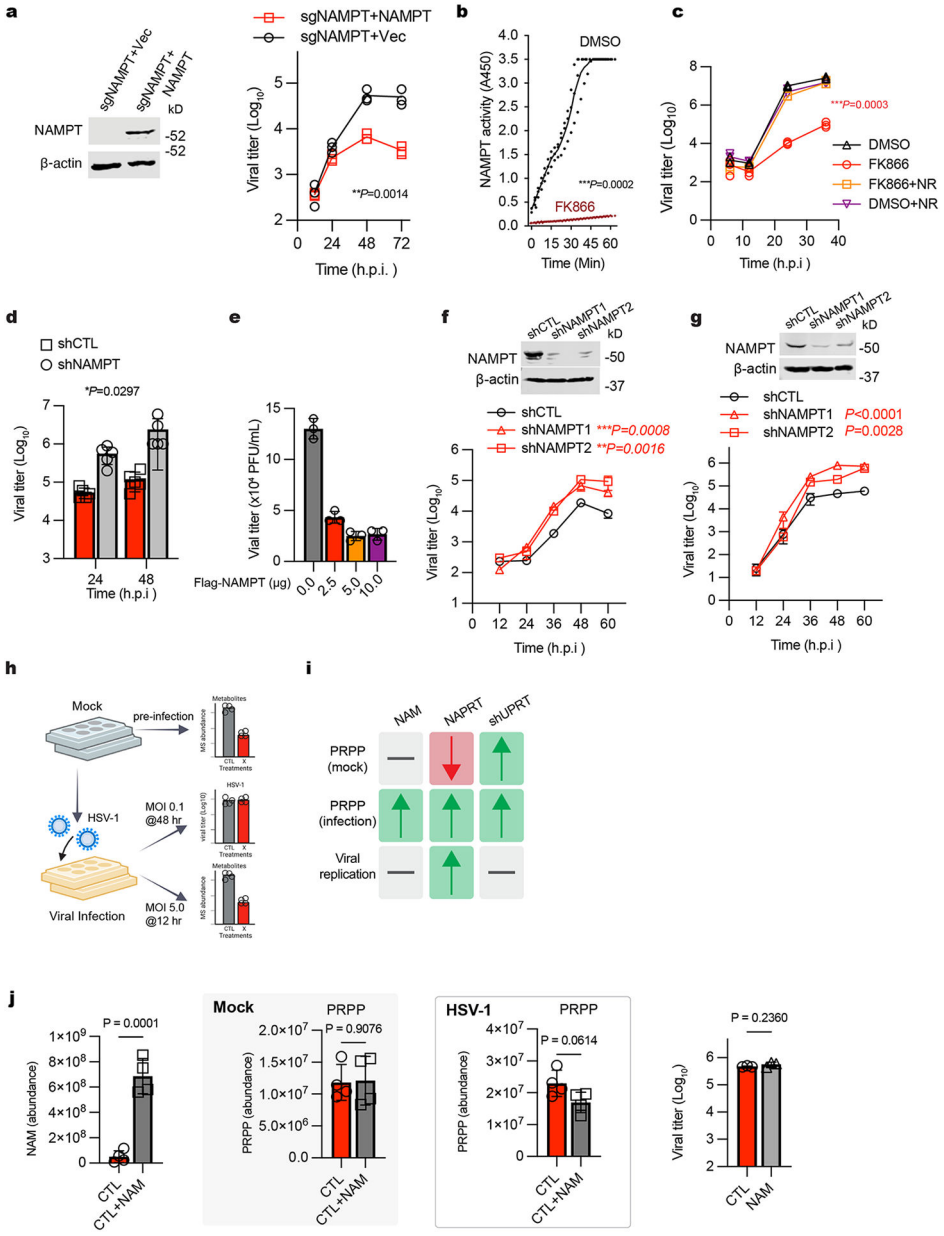

Extended Data Fig. 2 |. NAMPT restricts HSV-1 lytic replication.

a, HSV-1 growth curve in sgNAMPT HeLa cells reconstituted with NAMPT expression, n = 3, P = 0.0014. **b**, NAMPT enzymatic activity in NAD^+ synthesis was determined with or without FK866 (10 nM), n = 3. P = 0.0002. **c**, HSV-1 titer in HepG2 cells treated with

vehicle (DMSO) or FK866 (10 nM), with or without nicotinamide riboside (NR, 0.1 mM), n = 3, P = 0.0003 for FK866 versus DMSO. FK866 was added at 96 hours before HSV-1 infection and treatment was extended during infection. NR was added immediately before HSV-1 infection. **d**, HSV-1 titer in the medium of shCTL and shNAMPT HepG2 cells at MOI = 0.1 determined by plaque assay, n = 5, P = 0.0297. **e**, HSV-1 titer in the medium of 293 T cells that transiently express FLAG-NAMPT in increasing dose as indicated by plasmid amount at 24 h.p.i (MOI = 0.1), n = 3. **f-g**, Growth curve of HSV-1 in the medium of shCTL and shNAMPT mouse embryonic fibroblasts (MEFs) and human foreskin fibroblasts (HFF) at MOI = 0.1, with NAMPT knockdown validated by immunoblotting with indicated antibodies using whole cell lysates. **h-i**, Diagram (h) and summary (i) of PRPP levels and its effect on HSV-1 replication in HeLa cells by NAM, NAPRT expression or UPRT (UMP synthetase) depletion. **j**, HeLa cells, grown with exogenous NAM (0.1 mM), were mock- or HSV-1-infected as indicated in (h). PRPP were determined by LC-MS at 12 h.p.i. and viral titer in the medium was determined by plaque assay using Vero monolayer, n = 3 for viral titration, n = 4 for NAM and PRPP analysis. Diagram was created with Biorender.com. Statistical significance was calculated using two-way ANOVA for a, b, c, d, f, and g, unpaired two-tailed *t*-tests for j. Data are presented as mean values±SD. Graphics created with BioRender.com.

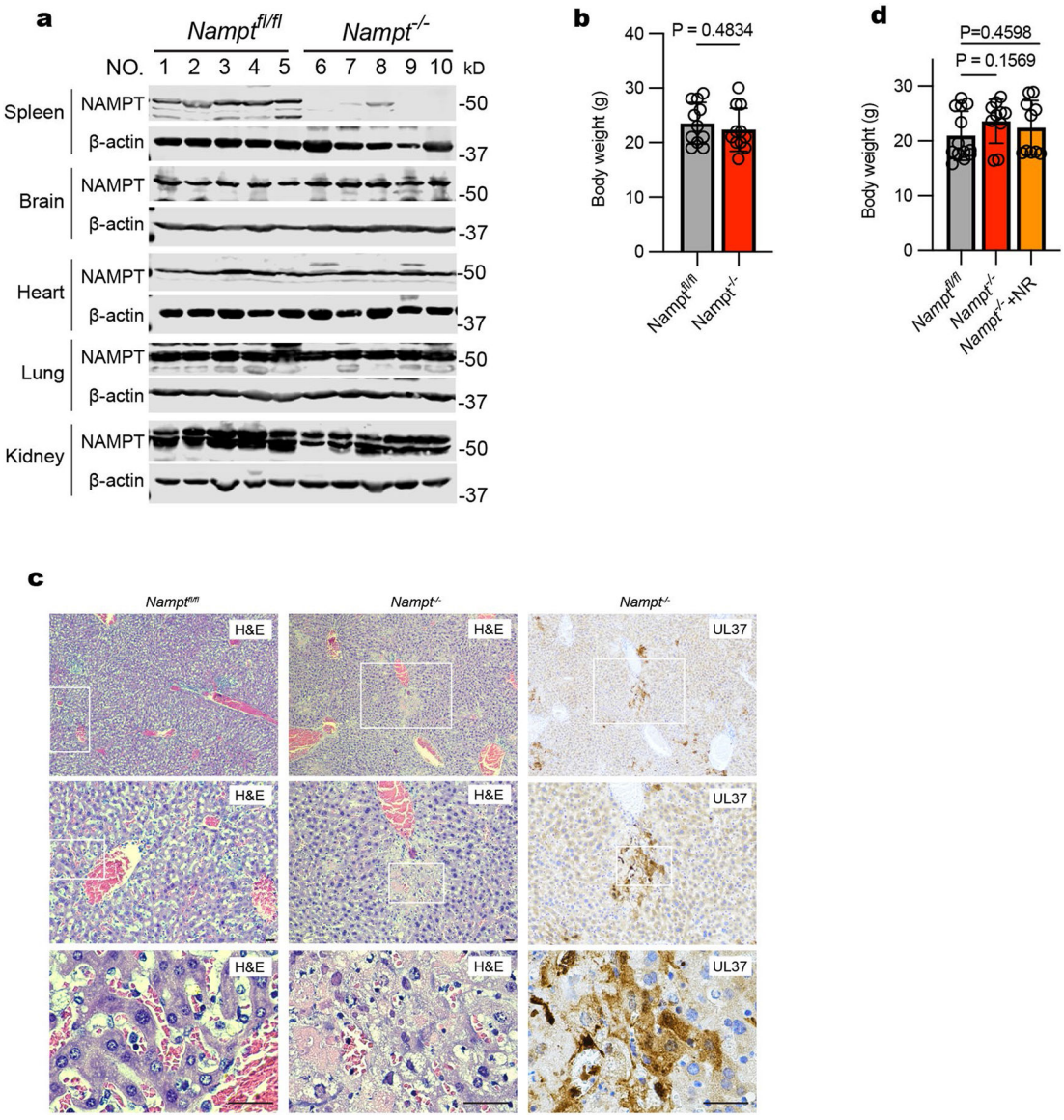

Extended Data Fig. 3 |. NAMPT restricts HSV-1 replication in mice.

a, Lysates of indicated tissues of wildtype and NAMPT-KO mice were analyzed by immunoblotting with indicated antibodies. **b**, Body weight of wildtype and NAMPT-KO mice was determined immediately before HSV-1 infection, n = 11. **c**, Hematolysin & Eosin (H&E) staining and UL37 immunohistochemistry staining of the liver of HSV-1-infected *Nampt*$^{fl/fl}$ and *Nampt*$^{-/-}$ mice, with boxed region shown below. Scale bars, 50 μm. **d**, Body weight of wildtype (n = 13), NAMPT-KO (n = 10) and NAMPT-KO mice with nicotinamide riboside (NR) supplementation via intraperitoneal injection (n = 10) was determined immediately before HSV-1 infection. Statistical significance was calculated using unpaired two-tailed *t*-tests for b and d. Data are presented as mean values±SD.

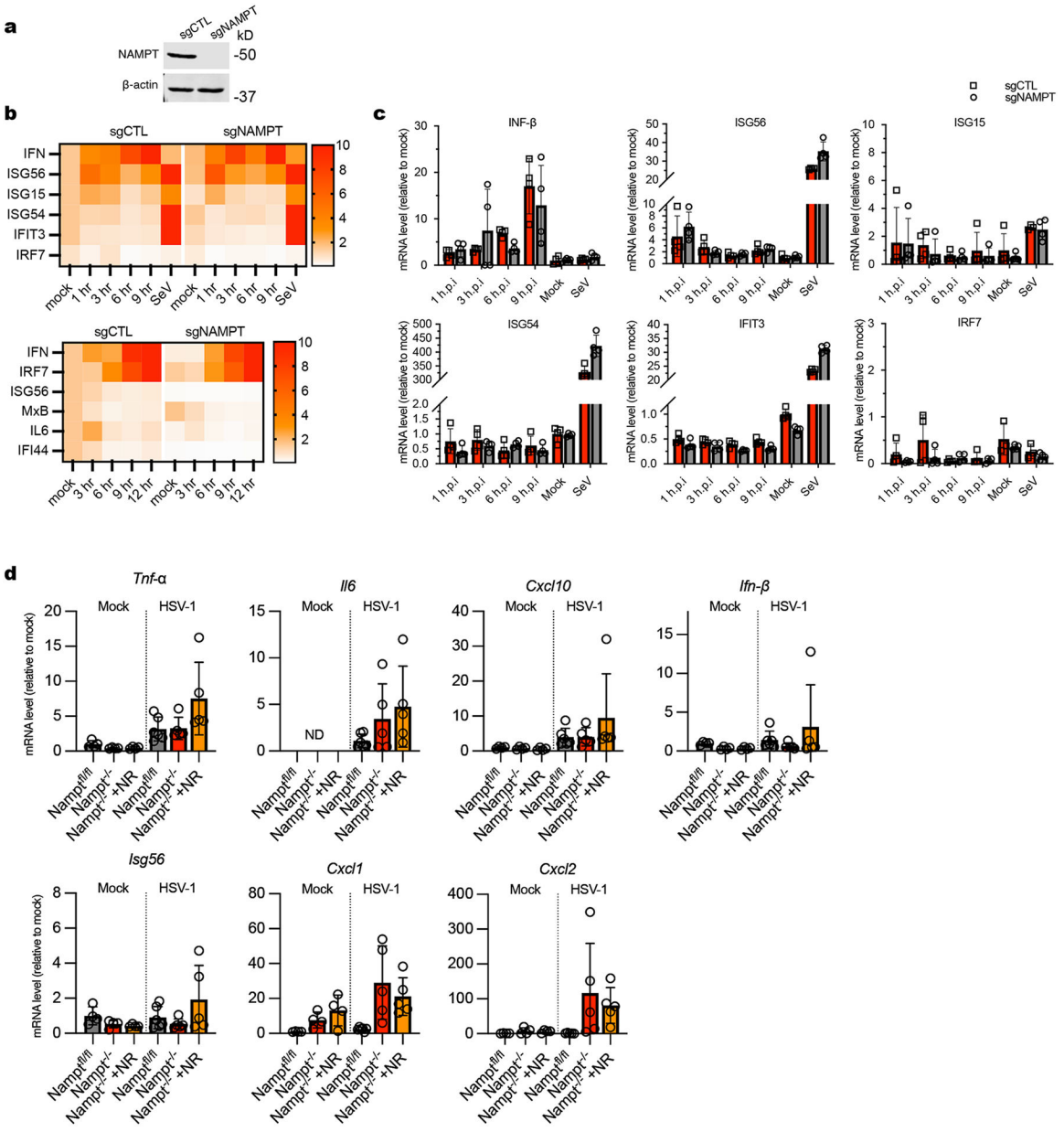

Extended Data Fig. 4 |. Loss of NAMPT does not compromise innate immune response against HSV-1.

a, NAMPT-KO in HepG2 cells was validated by immunoblotting with indicated antibodies using whole cell lysates. **b-c**, Heatmap of cytokine gene expression in sgCTL and sgNAMPT HepG2, with Sendai virus (SeV, 30 HA unit/ml) (b) and HeLa cells infected with HSV-1 (MOI = 2) (c). n = 3 for sgCTL HepG2 infected with Sendai virus for ISG15 and IRF7 analysis, n = 3 for sgCTL HepG2 mock group for IRF7 analysis, n = 4 for all the rest analyses. **d**, The mRNA of indicated inflammatory genes was determined by reverse transcription and real-time PCR using the liver of wildtype (n = 4 for mock, n = 6 for HSV-1 infection), NAMPT-KO (n = 4 for mock, n = 5 for HSV-1 infection) and NAMPT-KO mice with nicotinamide riboside (dose: 400 mg/kg/day, n = 4 for mock, n = 5 for HSV-1 infection)

at 3 days post-infection of HSV-1 (2×10^7 PFU, intravenous). ND, not detected. Data in c and d are presented as mean values±SD.

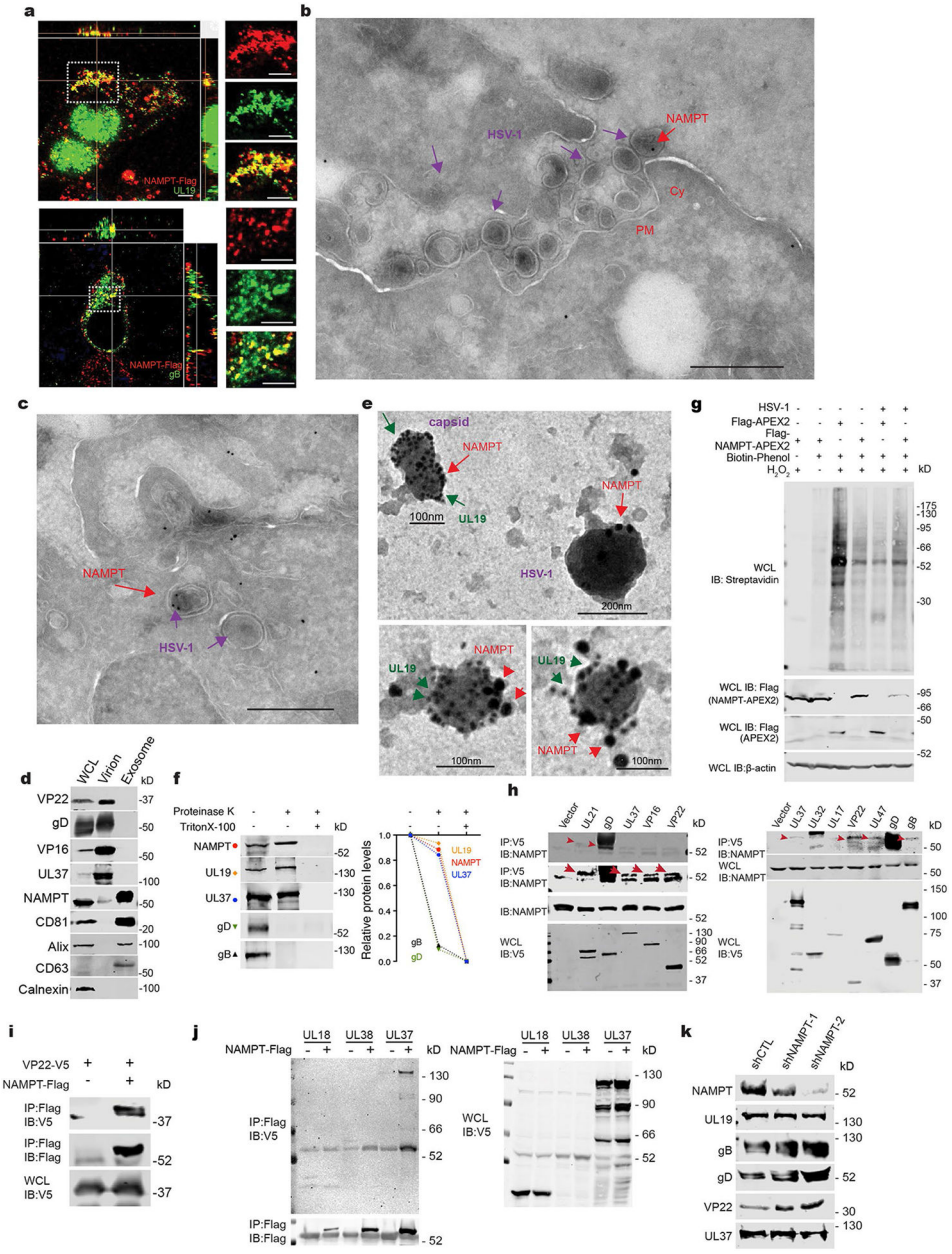

Extended Data Fig. 5 |. NAMPT is incorporated into HSV-1 virions.

a, Representative immunofluorescence images of HSV-1-infected sgNAMPT HeLa cells reconstituted with FLAG-NAMPT using antibodies to FLAG (NAMPT), UL19, and gB. Scale bars, 5 μm. **b-c**, Cryo-electron microscopy analysis of NAMPT in HSV-1-infected sgNAMPT HeLa cell reconstituted with HA-NAMPT. Scale bars, 500 nm. **d**, Purified HSV-1 virions, along with whole cell lysates and exosomes, were analyzed by immunoblotting with antibodies against known exosome markers and HSV-1 structural proteins. **e**, Transmission electron microscopy analysis of purified HSV-1 virions after

permeabilization with 1% Triton X-100 and immunogold-staining with antibodies to UL19 (10 nm gold) and HA (NAMPT, 25 nm gold). **f**, Top panels: Immunoblotting analysis of purified HSV-1 virions treated with protease K, in the absence or presence of Triton X-100 (1%), with antibodies to NAMPT and viral proteins. Bottom panel: Diagram of sensitivity to proteinase K of HSV-1 envelope glycoproteins, tegument protein UL37, and capsid protein UL19 with or without Triton X-100. Proteins were indicated by symbols with distinct shapes and colors. **g**, Immunoblotting analysis of whole cell lysates (WCL) of HeLa cells stably expressing APEX and NAMPT-APEX infected with HSV-1 for biotinylation assay, with H_2O_2 serves as a positive control. **h**, HSV-1 proteins, including UL21, gD, UL37, VP16, VP22, UL32, UL17, UL47, and gB precipitated with endogenous NAMPT in transfected 293 T cells. **i-j**, NAMPT interactions with VP22 (I), UL37, UL18, and UL38 (J) in transfected 293 T cells were analyzed by co-immunoprecipitation and immunoblotting. **k**, Immunoblotting analysis of HSV-1 structural proteins with indicated antibodies using virions produced from shCTL and shNAMPT HepG2 cells that were normalized against the UL19 capsid protein.

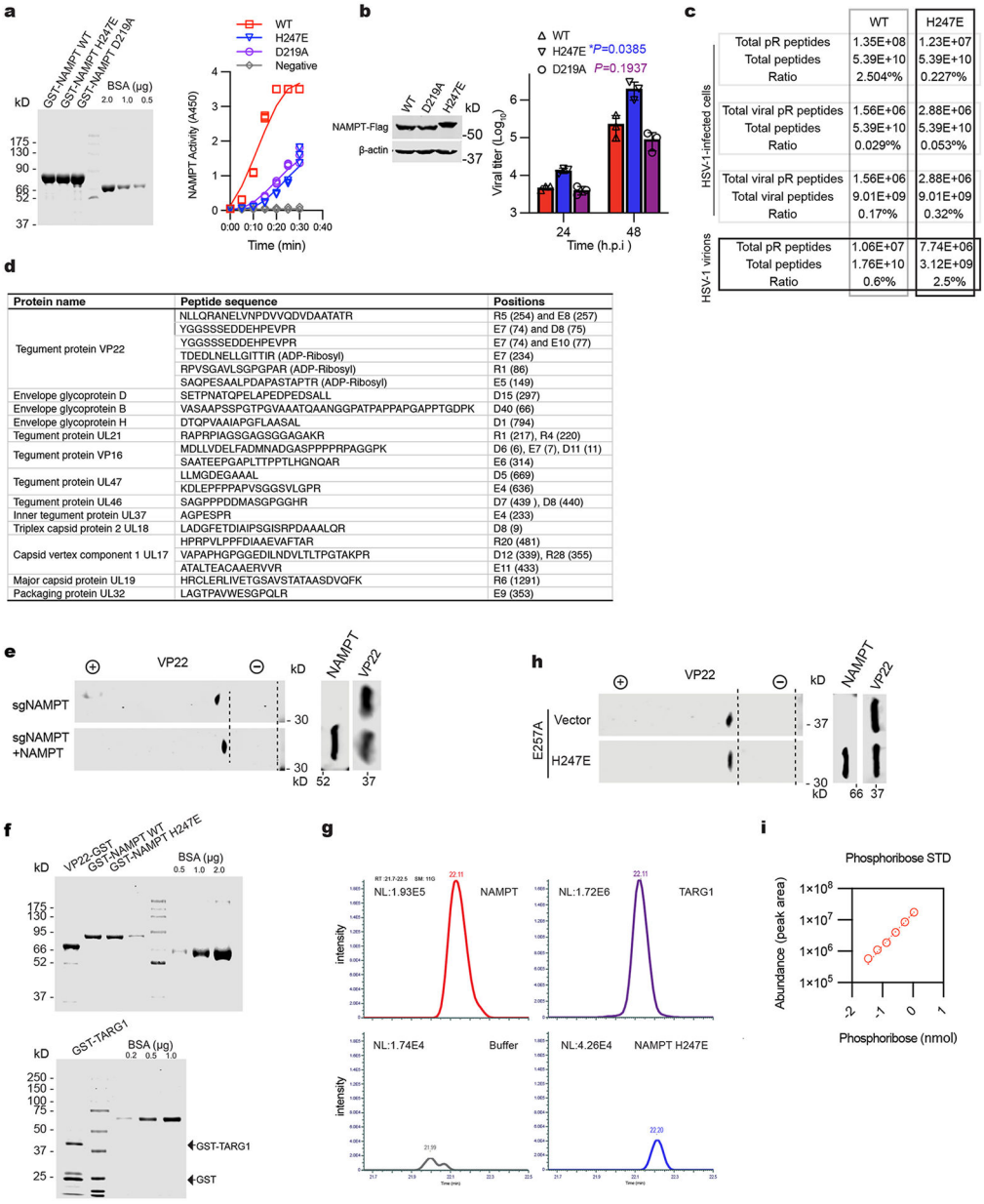

Extended Data Fig. 6 |. NAMPT is a protein phosphoribosylase.

a, Phosphoribosyltransferase activity in NAD^+ synthesis of NAMPT wildtype (WT), H247E and D219A that were purified from bacteria. NAMPT proteins purified to high homogeneity were validated by Coomassie staining and shown on the left. **b**, HSV-1 titer in sgNAMPT HeLa cells reconstituted with NAMPT WT, H247E and D219A mutants at 24 and 48 h.p.i., n = 3. Statistical significance was calculated using two-way ANOVA. Data are presented as mean values±SD. **c**, Quantification of the total phosphoribosylated peptides normalized to the total peptides (top panel), the total phosphoribosylated viral peptides normalized to the total peptides and total viral peptides (2^{nd} and 3^{rd} panel from top) in lysates of HeLa cells stably expressing wildtype NAMPT or the NAMPT-H247E mutant, and that of the phosphoribosylated viral peptides normalized to the total viral peptides of HSV-1

virions produced from HeLa cells expressing wildtype NAMPT or NAMPT-H247E (bottom panel). **d**, A list of identified phosphoribosylated and ADP-ribosylated (only in VP22) sites within their corresponding peptides, mapped to HSV-1 proteins. Numbers in parentheses indicate the corresponding phosphoribosylated residues within HSV-1 proteins. Please see Supplementary Fig. 1. **e**, Two-dimensional gel electrophoresis and immunoblotting analysis of VP22 in sgNAMPT 293 T cells and those reconstituted with NAMPT expression. **f**, Coomassie staining of purified GST-VP22, GST-NAMPT, GST-NAMPT-H247E (top panel) and GST-TARG1 (bottom panel). **g**, Detection of phosphoribose in reactions containing buffer, NAMPT, NAMPT-H247E, or TARG1 by LC-MS with GST-VP22 as the substrate. **h**, Two-dimensional gel electrophoresis and immunoblotting analysis of VP22-E257A in 293 T cells transiently expressing the NAMPT-H247E mutant with antibody against V5 (VP22). **i**, Phosphoribose in serial dilutions was determined by LC-MS, which serves as a standard for phosphoribose released from the NAMPT phosphoribosylase reaction. **j**, The phosphoribosylase activity of NAMPT H247E analyzed by released phosphoribose that is quantitatively determined by liquid chromatography-mass spectrometry. Statistical significance was calculated using unpaired two-tailed *t*-tests.

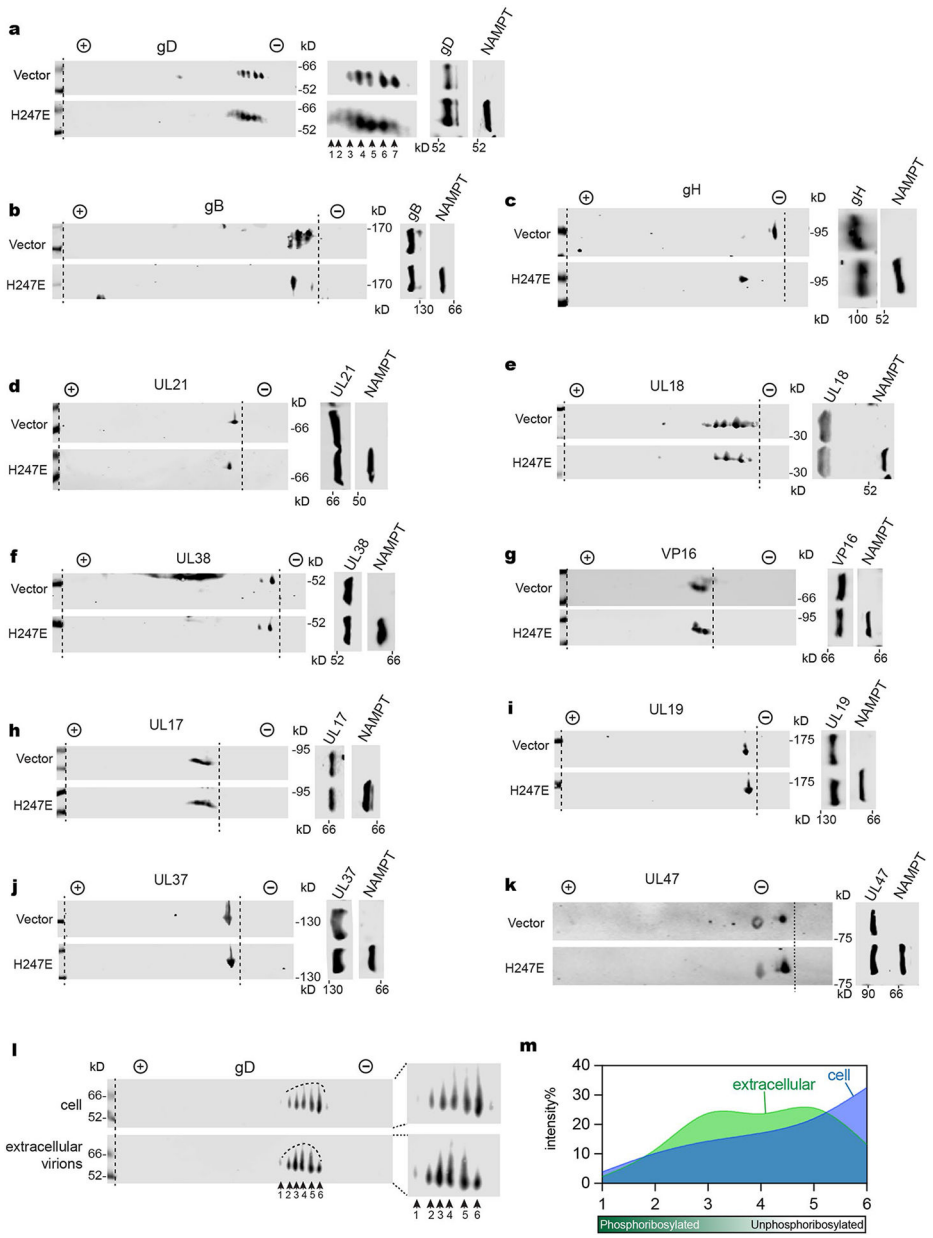

Extended Data Fig. 7 l. Phosphoribose of structural proteins promotes their virion incorporation.

a-k, Whole cell lysates of 293 T cells transiently expressing the NAMPT-H247E mutant and HSV-1 proteins, including gD (a), gB (b), gH (c), UL21(d), UL18 (e), UL38 (f), VP16 (g), UL17 (h), UL19 (i), UL37 (j), and UL47 (k), were analyzed by two-dimensional gel electrophoresis and immunoblotting with antibodies to the V5 epitope (HSV-1 proteins) and FLAG (NAMPT). **l-m**, Two-dimensional gel electrophoresis and immunoblotting analysis of purified intracellular and extracellular HSV-1 virions (produced from sgNAMPT 293 T cells) with antibodies to gD (l) and quantification by densitometry of gD species (m). Numbers at the bottom (a and l) and on x-axis (m) indicate the gD species with distinct charge status.

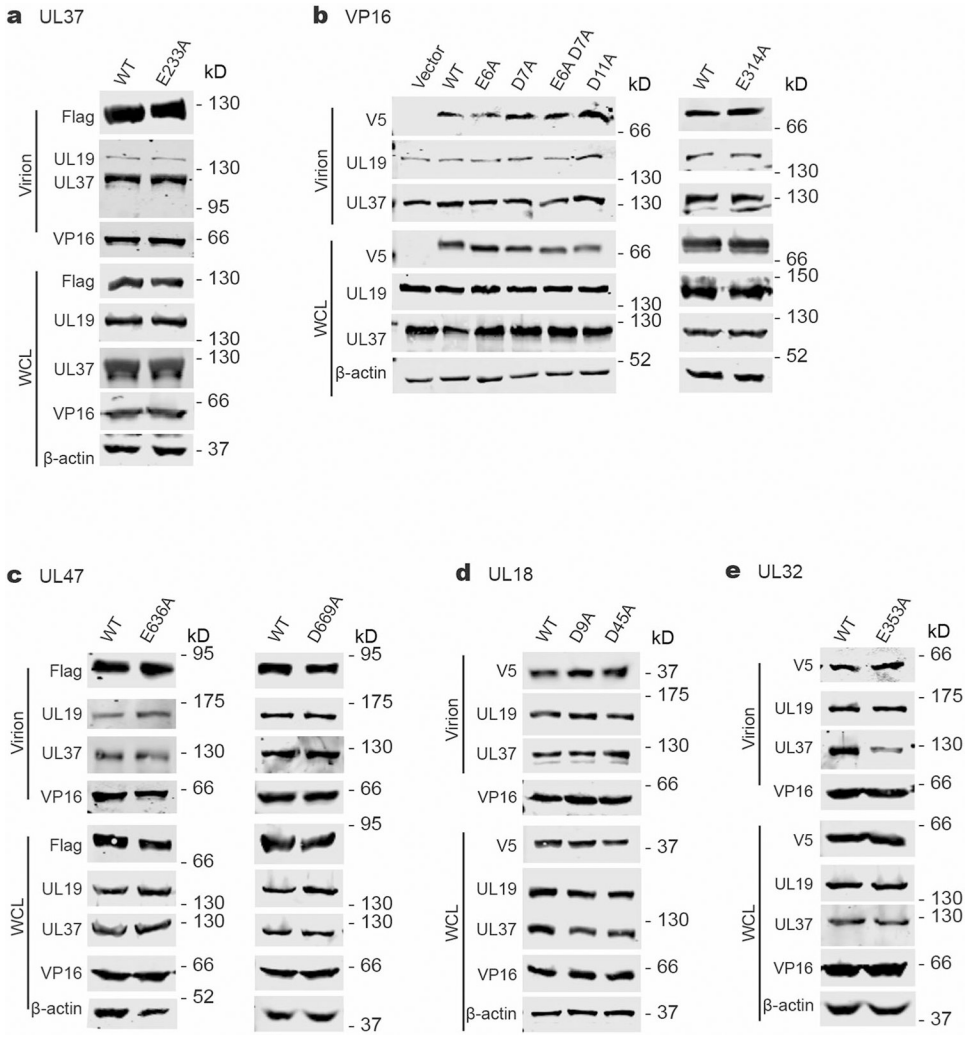

Extended Data Fig. 8 |. Virion incorporation of phosphoribosylation-resistant mutants of HSV-1 proteins.

a-e, Wild-type and phosphoribosylation-resistant mutants of HSV-1 proteins, including UL37 (a), VP16 (b), UL47 (c), UL18 (d), and UL32 (e), incorporated in extracellular HSV-1 virions and expressed in HSV-1-infected cells were analyzed by immunoblotting with indicated antibodies. All HSV-1 proteins were tagged with either the V5 epitope (VP16, UL18 AND UL32) or FLAG epitope (UL37 and UL47).

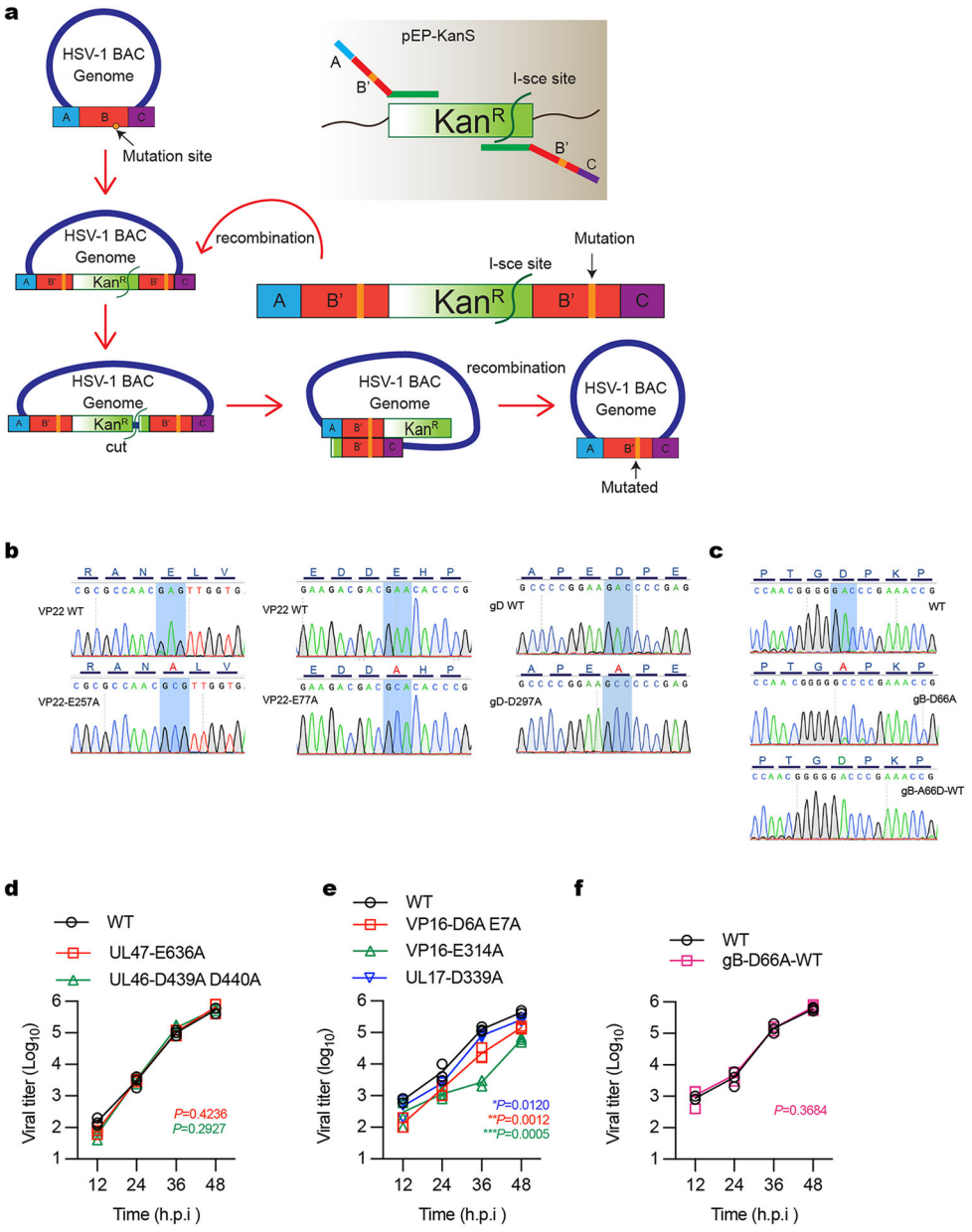

Extended Data Fig. 9 |. Functional characterization of phosphoribosylation in HSV-1 replication using recombinant HSV-1 carrying phosphoribosylation-resistant mutations.

a, Schematic illustration of engineering recombinant HSV-1 using the bacteria artificial chromosome (BAC) system. **b**, Mutations engineered in the HSV-1 genome were validated by sequencing (right panels). **c**, Mutation of gB-D66A and -A66D (revertant) in the HSV-1 genome was confirmed by sequencing. **d-e**, Growth curve of HSV-1 containing phosphoribosylation-resistant mutants of UL46 (D439, 440 A), UL47 (E636A) (**d**), VP16 (D6A, E7A, D314A) and UL17 (D339A) (**e**) in HepG2 cells (MOI = 0.1) was determined by plaque assays using Vero cells. **f**, Growth curve of parental wildtype (WT) HSV-1 and recombinant HSV-1 carrying gB-A66D (revertant) in HepG2 cells (MOI = 0.1) was

determined by plaque assay using Vero cells. Statistical significance was calculated using two-way ANOVA.

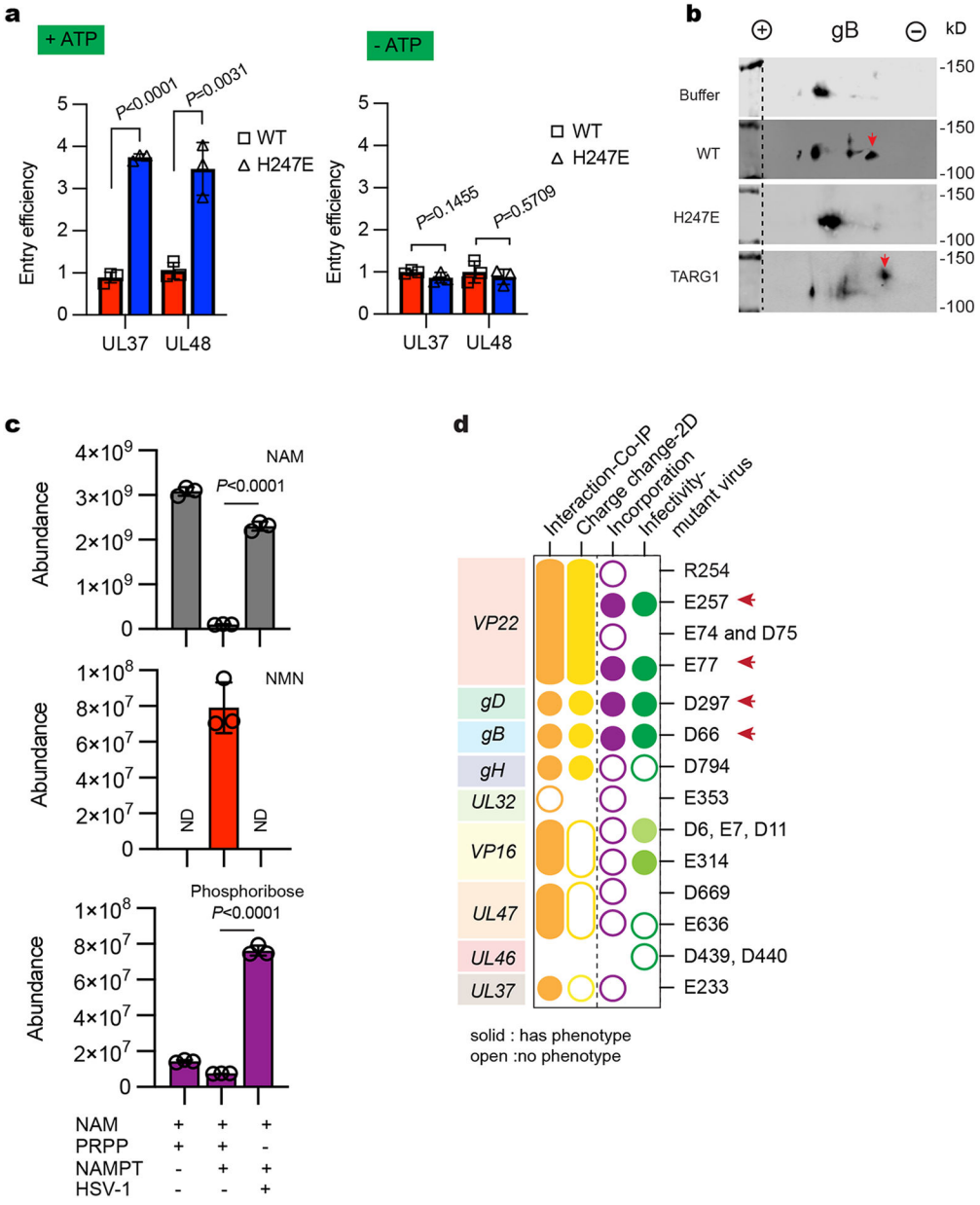

Extended Data Fig. 10 |. Phosphoribose of structural proteins promotes HSV-1 entry and replication.

a, Entry analysis of HSV-1 virions treated with NAMPT or NAMPT-H247E, with or without ATP (2 mM), n = 3. Statistical significance was calculated using unpaired two-tailed *t*-tests, $P < 0.0001$ (+ATP, UL37), $P = 0.0031$ (+ATP, UL48), $P = 0.1455$ (−ATP, UL37), $P = 0.5709$ (−ATP, UL48). **b**, Two-dimensional gel electrophoresis and immunoblotting analysis of HSV-1 virions treated with wildtype NAMPT (WT), the NAMPT-H247E mutant or TARG1 with antibody against gB. Red arrows indicate the new species produced by NAMPT or TARG1 treatment. **c**, Quantification of NAM, NMN and phosphoribose in the supernatant

of the in vitro phosphoribosylase reactions by mass spectrometry, n = 3. Statistical significance was calculated using unpaired two-tailed *t*-tests, $P < 0.0001$ for NAMPT + HSV-1 group versus NAMPT + PRPP group in NAM and phosphoribose analysis. ND, not detected. **d**, Summary of biochemical and functional characterization of the site-specific phosphoribosylation of HSV-1 proteins. Red arrows indicate the residues whose phosphoribosylation-resistant mutations displayed significant effect on HSV-1 infection. Intensity of colour indicates the degree of effect and open circles indicate no phenotype. Statistical significance was calculated using unpaired two-tailed Student's *t*-tests and two-way ANOVA analysis. Data in a and c are presented as mean values±SD.

Supplementary Material

Refer to Web version on PubMed Central for supplementary material.

Acknowledgements

We thank S.-I. Imai (Washington University) for providing the *Nampt*$^{fl/fl}$ mice, S. Petteri (Stanford University) and N. Graham (University of Southern California) for LC–MS techniques, J. Hao (Poochon Scientific) for APEX-related protein identification, W. Beatty (Washington University) for electron microscopy analysis, W. Yuan (University of Southern California), D. Knipe (Harvard Medical School) and R. Longnecker (Northwestern University) for providing HSV-1 plasmids, J. Zhao (Cleveland Clinic Foundation) for guidance on generating HSV-1 mutant viruses, G. Cohen (University of Pennsylvania) for anti-gH antibody, C. Zhen (University of Calgary) for anti-VP22 antibody, B. Lomenick (CalTech) for processing MS samples, and N. Graham (University of Southern California) and S. Pitteri (Stanford University) for assistance on mass spectrometry analysis. We are grateful to Y. Zhou, S. Rice, J. Carriere and J. Xiao for their assistance. This work was partly supported by a startup fund from the Herman Ostrow School of Dentistry of the University of Southern California and grants from the National Institutes of Health (AG070904, CA285192 and AI180537) and Infectious Disease Society of America Foundation (Microbial Pathogenesis in AD) (P.F.) and National Natural Science Foundation of China (81821002) (C.H.).

Data availability

All raw datasets used for phosphoribosylated peptide analysis can be found in the PRIDE public repository under project accession number PXD050684. All source data supporting the main figures and extended data figures are published within the paper. Source data are provided with this paper.

References

1. Girdhar K. et al. Viruses and metabolism: the effects of viral infections and viral insulins on host metabolism. Annu. Rev. Virol 8, 373–391 (2021). [PubMed: 34586876]
2. Schneider WM, Chevillotte MD & Rice CM Interferon-stimulated genes: a complex web of host defenses. Annu. Rev. Immunol 32, 513–545 (2014). [PubMed: 24555472]
3. Sadler AJ & Williams BR Interferon-inducible antiviral effectors. Nat. Rev. Immunol 8, 559–568 (2008). [PubMed: 18575461]
4. Lahouassa H. et al. SAMHD1 restricts the replication of human immunodeficiency virus type 1 by depleting the intracellular pool of deoxynucleoside triphosphates. Nat. Immunol 13, 223–228 (2012). [PubMed: 22327569]
5. Gizzi AS et al. A naturally occurring antiviral ribonucleotide encoded by the human genome. Nature 558, 610–614 (2018). [PubMed: 29925952]
6. Liu SY et al. Interferon-inducible cholesterol-25-hydroxylase broadly inhibits viral entry by production of 25-hydroxycholesterol. Immunity 38, 92–105 (2013). [PubMed: 23273844]

7. Verdin E. NAD^+ in aging, metabolism, and neurodegeneration. Science 350, 1208–1213 (2015). [PubMed: 26785480]
8. Yoshino J, Baur JA & Imai SI NAD^+ intermediates: the biology and therapeutic potential of NMN and NR. Cell Metab. 27, 513–528 (2018). [PubMed: 29249689]
9. Lautrup S, Sinclair DA, Mattson MP & Fang EF NAD^+ in brain aging and neurodegenerative disorders. Cell Metab. 30, 630–655 (2019). [PubMed: 31577933]
10. Huang D & Kraus WL The expanding universe of PARP1-mediated molecular and therapeutic mechanisms. Mol. Cell 82, 2315–2334 (2022). [PubMed: 35271815]
11. Groslambert J, Prokhorova E & Ahel I ADP-ribosylation of DNA and RNA. DNA Repair (Amst.) 105, 103144 (2021). [PubMed: 34116477]
12. Challa S. et al. Ribosome ADP-ribosylation inhibits translation and maintains proteostasis in cancers. Cell 184, 4531–4546.e26 (2021). [PubMed: 34314702]
13. Palazzo L. et al. ENPP1 processes protein ADP-ribosylation in vitro. FEBS J. 283, 3371–3388 (2016). [PubMed: 27406238]
14. Thirawatananond P. et al. Structural analyses of NudT16–ADP-ribose complexes direct rational design of mutants with improved processing of poly(ADP-ribosyl)ated proteins. Sci. Rep 9, 5940 (2019). [PubMed: 30976021]
15. Katsyuba E, Romani M, Hofer D & Auwerx J NAD^+ homeostasis in health and disease. Nat. Metab 2, 9–31 (2020). [PubMed: 32694684]
16. Garten A. et al. Physiological and pathophysiological roles of NAMPT and NAD metabolism. Nat. Rev. Endocrinol 11, 535–546 (2015). [PubMed: 26215259]
17. Yoshida M. et al. Extracellular vesicle-contained eNAMPT delays aging and extends lifespan in mice. Cell Metab. 30, 329–342.e5 (2019). [PubMed: 31204283]
18. Smith GA Assembly and egress of an alphaherpesvirus clockwork. Adv. Anat. Embryol. Cell Biol 223, 171–193 (2017). [PubMed: 28528444]
19. Laine RF et al. Structural analysis of herpes simplex virus by optical super-resolution imaging. Nat. Commun 6, 5980 (2015). [PubMed: 25609143]
20. Stremlau M. et al. The cytoplasmic body component TRIM5α restricts HIV-1 infection in Old World monkeys. Nature 427, 848–853 (2004). [PubMed: 14985764]
21. Dasgupta S. et al. Metabolic enzyme PFKFB4 activates transcriptional coactivator SRC-3 to drive breast cancer. Nature 556, 249–254 (2018). [PubMed: 29615789]
22. Zhao J. et al. Deamidation shunts RelA from mediating inflammation to aerobic glycolysis. Cell Metab. 31, 937–955.e7 (2020). [PubMed: 32325032]
23. Wang T. et al. Structure of Nampt/PBEF/visfatin, a mammalian NAD^+ biosynthetic enzyme. Nat. Struct. Mol. Biol 13, 661–662 (2006). [PubMed: 16783373]
24. Daniels CM, Ong SE & Leung AKL ADP-Ribosylated peptide enrichment and site identification: the phosphodiesterase-based method. Methods Mol. Biol 1608, 79–93 (2017). [PubMed: 28695505]
25. Matic I, Ahel I & Hay RT Reanalysis of phosphoproteomics data uncovers ADP-ribosylation sites. Nat. Methods 9, 771–772 (2012). [PubMed: 22847107]
26. Zhang Y, Wang J, Ding M & Yu Y Site-specific characterization of the Asp- and Glu-ADP-ribosylated proteome. Nat. Methods 10, 981–984 (2013). [PubMed: 23955771]
27. Revollo JR, Grimm AA & Imai S The NAD biosynthesis pathway mediated by nicotinamide phosphoribosyltransferase regulates Sir2 activity in mammalian cells. J. Biol. Chem 279, 50754–50763 (2004). [PubMed: 15381699]
28. Connolly SA, Jardetzky TS & Longnecker R The structural basis of herpesvirus entry. Nat. Rev. Microbiol 19, 110–121 (2021). [PubMed: 33087881]
29. Chesnokova LS, Jiang R & Hutt-Fletcher LM Viral entry. Curr. Top. Microbiol. Immunol 391, 221–235 (2015). [PubMed: 26428376]
30. Schoggins JW et al. A diverse range of gene products are effectors of the type I interferon antiviral response. Nature 472, 481–485 (2011). [PubMed: 21478870]
31. Van den Bergh R. et al. Transcriptome analysis of monocyte–HIV interactions. Retrovirology 7, 53 (2010). [PubMed: 20546557]

32. Li J et al. Antiviral activity of a purine synthesis enzyme reveals a key role of deamidation in regulating protein nuclear import. Sci. Adv 5, eaaw7373 (2019). [PubMed: 31633017]
33. He S. et al. Viral pseudo-enzymes activate RIG-I via deamidation to evade cytokine production. Mol. Cell 58, 134–146 (2015). [PubMed: 25752576]
34. Pan C, Li B & Simon MC Moonlighting functions of metabolic enzymes and metabolites in cancer. Mol. Cell 81, 3760–3774 (2021). [PubMed: 34547237]
35. Weixler L. et al. ADP-ribosylation of RNA and DNA: from in vitro characterization to in vivo function. Nucleic Acids Res. 49, 3634–3650 (2021). [PubMed: 33693930]
36. Munnur D. et al. Reversible ADP-ribosylation of RNA. Nucleic Acids Res. 47, 5658–5669 (2019). [PubMed: 31216043]
37. Wang X. et al. Deletion of *Nampt* in projection neurons of adult mice leads to motor dysfunction, neurodegeneration, and death. Cell Rep. 20, 2184–2200 (2017). [PubMed: 28854367]
38. Zhang LQ et al. Metabolic and molecular insights into an essential role of nicotinamide phosphoribosyltransferase. Cell Death Dis. 8, e2705 (2017). [PubMed: 28333140]
39. Bhogaraju S. et al. Phosphoribosylation of ubiquitin promotes serine ubiquitination and impairs conventional ubiquitination. Cell 167, 1636–1649.e13 (2016). [PubMed: 27912065]
40. Yoon MJ et al. SIRT1-mediated eNAMPT secretion from adipose tissue regulates hypothalamic NAD^+ and function in mice. Cell Metab. 21, 706–717 (2015). [PubMed: 25921090]
41. Trammell SA et al. Nicotinamide riboside is uniquely and orally bioavailable in mice and humans. Nat. Commun 7, 12948 (2016). [PubMed: 27721479]
42. Chen S. et al. Genome-wide CRISPR screen in a mouse model of tumor growth and metastasis. Cell 160, 1246–1260 (2015). [PubMed: 25748654]
43. Dai X & Zhou ZH Purification of herpesvirus virions and capsids. Bio. Protoc 4, e1193 (2014).
44. Cardone G. et al. The UL36 tegument protein of herpes simplex virus 1 has a composite binding site at the capsid vertices. J. Virol 86, 4058–4064 (2012). [PubMed: 22345483]
45. Cheng Q, Shi X & Zhang Y Reprogramming exosomes for immunotherapy. Methods Mol. Biol 2097, 197–209 (2020). [PubMed: 31776927]
46. Langelier CR et al. Biochemical characterization of a recombinant TRIM5α protein that restricts human immunodeficiency virus type 1 replication. J. Virol 82, 11682–11694 (2008). [PubMed: 18799573]
47. Lundgren DH, Hwang SI, Wu L & Han DK Role of spectral counting in quantitative proteomics. Expert Rev. Proteomics 7, 39–53 (2010). [PubMed: 20121475]
48. Daniels CM, Ong SE & Leung AK Phosphoproteomic approach to characterize protein mono- and poly(ADP-ribosyl) ation sites from cells. J Proteome Res. 13, 3510–3522 (2014). [PubMed: 24920161]
49. Zhang RY et al. A fluorometric assay for high-throughput screening targeting nicotinamide phosphoribosyltransferase. Anal. Biochem 412, 18–25 (2011). [PubMed: 21211508]
50. Gardell SJ et al. Boosting NAD^+ with a small molecule that activates NAMPT. Nat. Commun 10, 3241 (2019). [PubMed: 31324777]
51. Brulois KF et al. Construction and manipulation of a new Kaposi's sarcoma-associated herpesvirus bacterial artificial chromosome clone. J. Virol 86, 9708–9720 (2012). [PubMed: 22740391]

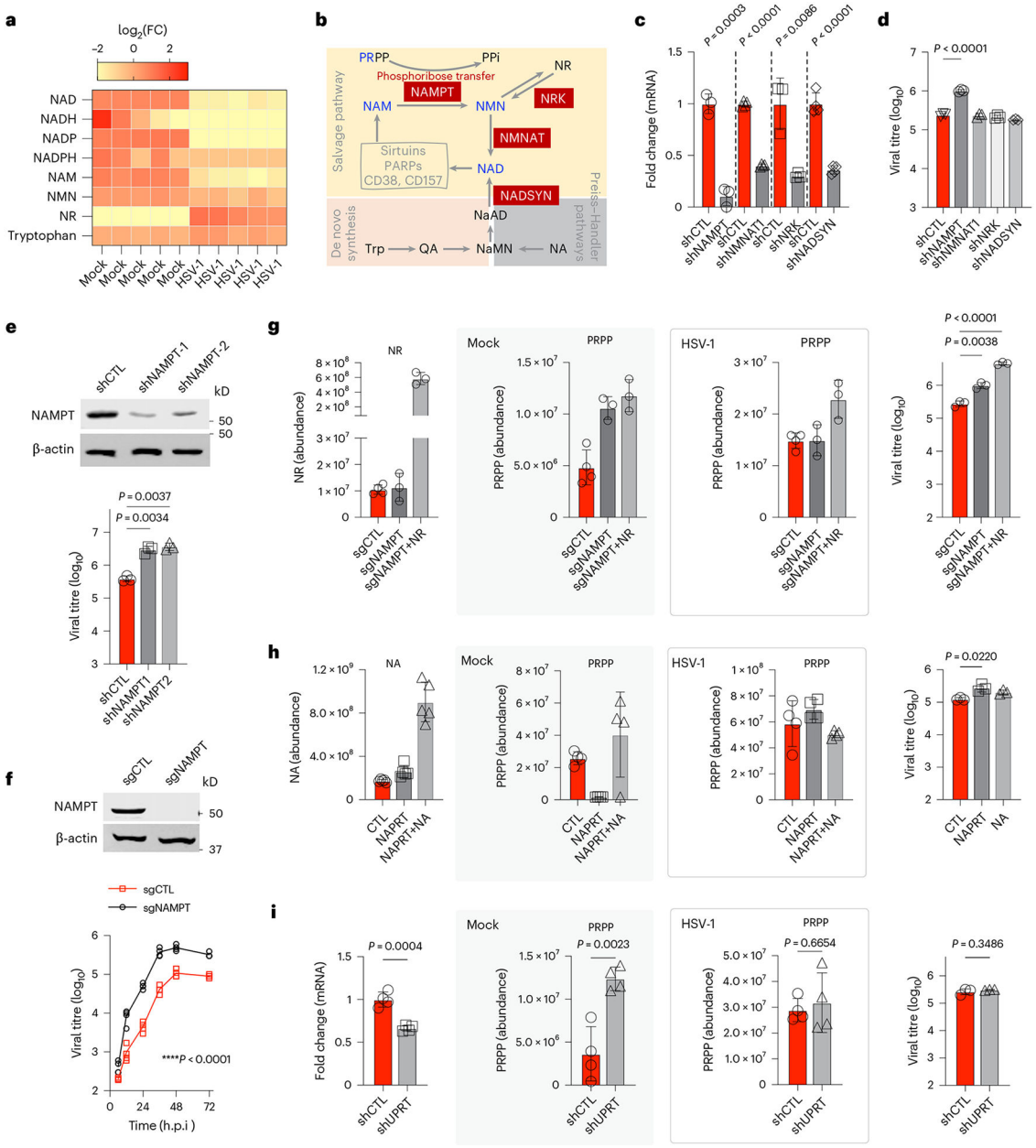

Fig. 1 | NAMPT restricts HSV-1 lytic replication.

a, Heatmap of the NAD$^+$-related metabolites in HSV-1-infected HepG2 cells (multiplicity of infection (MOI) = 2, 12 h post infection (h.p.i.)). **b**, Schematic illustration of the NAD$^+$ synthesis pathways. **c**, Knockdown of NAMPT ($n = 3$, $P = 0.0003$), NMNAT1 ($n = 4$, $P < 0.0001$), NRK ($n = 3$, $P = 0.0086$) or NADSYN ($n = 3$, $P < 0.0001$) in 293T cells validated by RT–qPCR using total RNA. **d**, HSV-1 titre in the medium of 293T cells with depletion of NAMPT ($n = 3$, $P < 0.0001$), NMNAT1 ($n = 3$), NRK ($n = 3$) or NADSYN ($n = 3$). **e**, HSV-1 titres in control (shCTL) and NAMPT-knockdown (shNAMPT) HeLa cells supplemented with NR (0.1 mM), $n = 3$, $P = 0.0034$ for shNAMPT1 versus shCTL, $P = 0.0037$ for shNAMPT2 versus shCTL. **f**,**g**, HSV-1 growth curve in control (sgCTL) and NAMPT-KO (sgNAMPT) HeLa cells supplemented with NR (0.1 mM), $n = 3$, $P < 0.0001$. Intracellular

PRPP was determined by LC–MS at 12 h.p.i., $n = 4$ for shCTL, $n = 3$ for sgNAMPT and sgNAMPT + NR (**f**). Viral titre in the medium at 48 h.p.i was determined by plaque assay using a Vero monolayer, $n = 3$, $P = 0.0038$ for sgNAMPT versus shCTL and $P < 0.0001$ for sgNAMPT + NR versus shCTL (**g**). **h**,**i**, HeLa cells were infected with lentivirus expressing NAPRT (**h**) or shUPRT (**i**). HeLa cells were mock-infected or HSV-1-infected as indicated in (**a**). Intracellular PRPP was determined by LC–MS at 12 h.p.i ($n = 4$), and viral titre in the medium was determined by plaque assay using a Vero monolayer ($n = 3$, $P = 0.022$ for shNAPRT versus shCTL; $P = 0.3486$ for shUPRT versus shCTL). Statistical significance was calculated using unpaired two-tailed *t*-tests for **c**, **d**, **e**, **g**, **h** and **i**; two-way ANOVA for **f**. Data are presented as mean values ± s.d. in **d**, **e**, **g**, **i** and **j**.

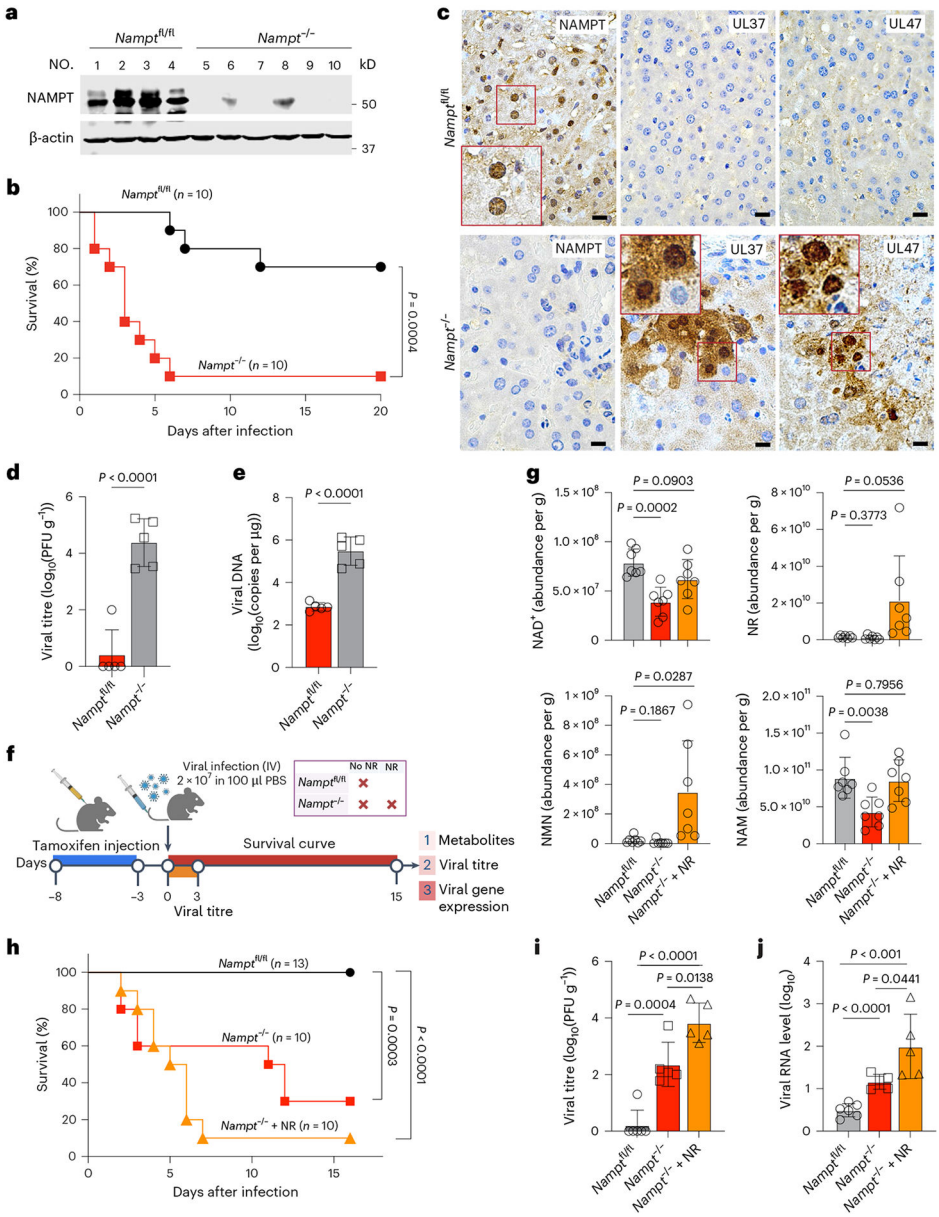

Fig. 2 |. NAMPT restricts HSV-1 lytic replication in mice.

a, Immunoblotting analysis of the liver of *Nampt*$^{fl/fl}$ and *Nampt*$^{-/-}$ mice infected with HSV-1, with indicated antibodies. **b–e**, Age- (12–14-week-old) and gender-matched *Nampt*$^{fl/fl}$ and *Nampt*$^{-/-}$ mice were infected with HSV-1 (5×10^7 PFU, intravenous injection) and mouse survival was recorded (**b**), immunohistology was performed with antibodies against NAMPT and HSV-1 antigens (UL37 and UL47) (**c**), HSV-1 load was determined by plaque assays using liver homogenates, $n = 5$, $P < 0.0001$ (**d**) and viral genome copy number was determined by real-time PCR using extracted total DNA, $n = 5$, $P < 0.0001$ (**e**). **f–j**, Diagram of the experimental design involving NAMPT deletion via tamoxifen injection, HSV-1 infection, mouse survival, HSV-1 replication and host immune response (**f**). Age-matched (12–14-week-old) and gender-matched *Nampt*$^{fl/fl}$ and *Nampt*$^{-/-}$ mice were used in these experiments. NR was injected (400 mg kg^{-1} d^{-1}) intraperitoneally

at the time of tamoxifen induction. The NAD^+-related metabolites (**g**) in the liver of wild-type ($n = 7$), NAMPT-KO ($n = 7$) and NAMPT-KO with NR supplementation ($n = 7$) were determined immediately before HSV-1 infection. Mouse survival was recorded after HSV-1 infection (2×10^7 PFU, intravenous), $P = 0.0003$ for *Nampt*$^{-/-}$ versus *Nampt*$^{fl/fl}$, $P < 0.0001$ for *Nampt*$^{-/-}$ + NR versus *Nampt*$^{fl/fl}$ (**h**). HSV-1 replication was determined by plaque assay, $n = 6$ for *Nampt*$^{fl/fl}$, $n = 5$ for *Nampt*$^{-/-}$ and *Nampt*$^{-/-}$ + NR; $P = 0.0004$ for *Nampt*$^{-/-}$ versus *Nampt*$^{fl/fl}$, $P < 0.0001$ for *Nampt*$^{-/-}$ + NR versus *Nampt*$^{fl/fl}$, $P = 0.0138$ for *Nampt*$^{-/-}$ + NR versus *Nampt*$^{-/-}$ (**i**). Viral gene expression by reverse transcription followed by real-time PCR, $n = 6$ for *Nampt*$^{fl/fl}$, $n = 5$ for *Nampt*$^{-/-}$ and *Nampt*$^{-/-}$ + NR; $P < 0.0001$ for *Nampt*$^{-/-}$ versus *Nampt*$^{fl/fl}$, $P < 0.0001$ for *Nampt*$^{-/-}$ + NR versus *Nampt*$^{fl/fl}$, $P = 0.0441$ for *Nampt*$^{-/-}$ + NR versus *Nampt*$^{-/-}$ (**j**). Scale bar, 10 μm. Statistical significance was calculated using the log-rank test for mouse survival data (in **b** and **h**), unpaired two-tailed *t*-tests for **d**, **e**, **g**, **I** and **j**. Data are presented as mean values; error bars, s.d. in **d**, **e**, **g**, **i** and **j**. Graphics created with BioRender.com.

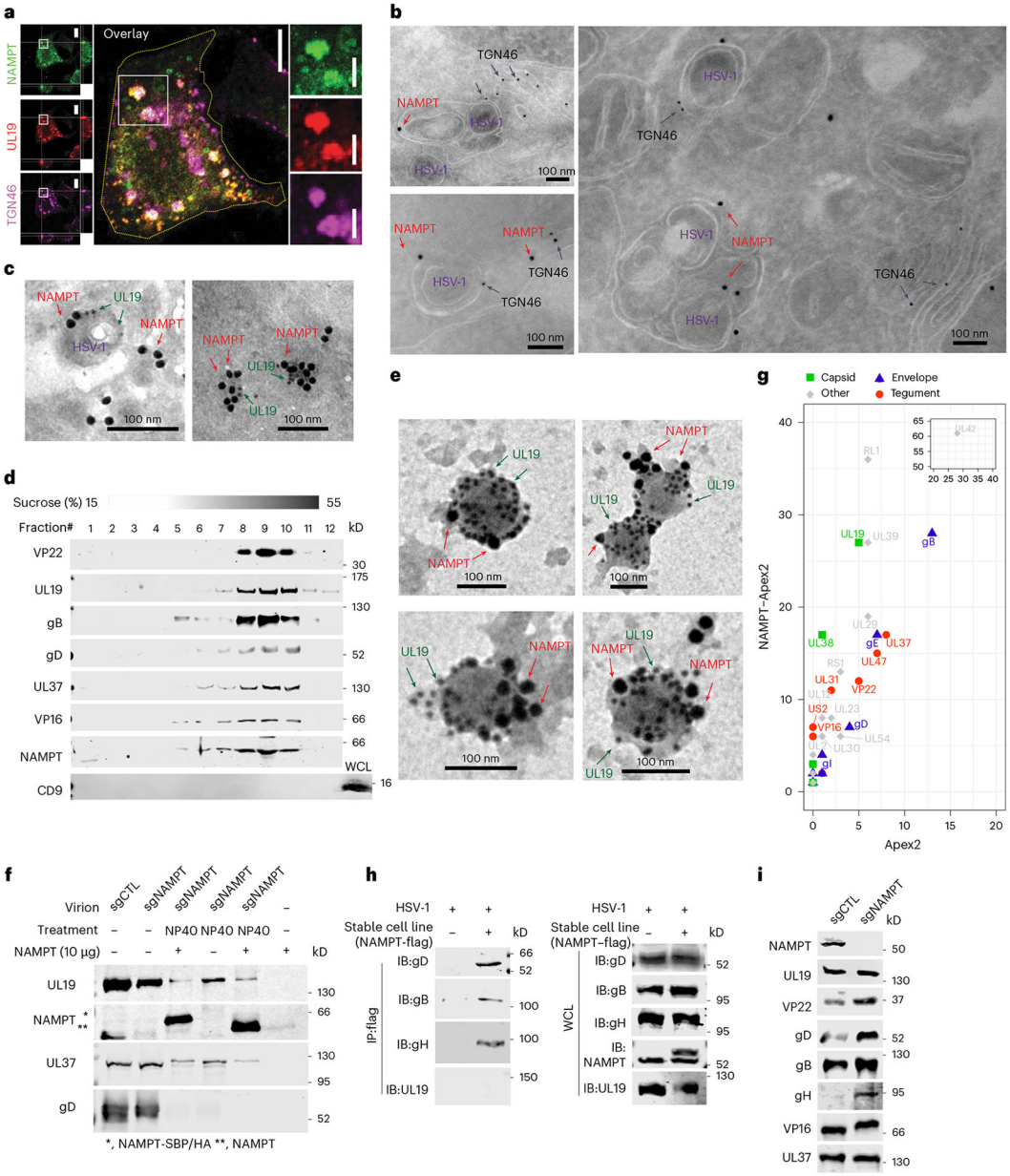

Fig. 3 | NAMPT is packaged in HSV-1 virions.

a–**c**, sgNAMPT HeLa cells reconstituted with HA–NAMPT were infected with HSV-1 (MOI = 2) for 12 h. Immunofluorescence image of HSV-1-infected HeLa cells with antibodies to HA (NAMPT), UL19 and TGN46, with boxed region amplified and shown on the right (**a**). Immunogold staining followed by electron microscopy analysis with antibody against HA (NAMPT, 25 nm gold) and TGN46 (10 nm gold) (**b**) or HA (NAMPT, 25 nm gold) and UL19 (10 nm gold) (**c**). **d**, Immunoblotting analysis of fractions of sucrose gradient ultracentrifugation with indicated antibodies. WCL, whole cell lysate. **e**, Transmission electron microscopy analysis of purified HSV-1 virions after immunogold staining with antibodies to UL19 (10 nm gold) and HA (NAMPT, 25 nm gold). **f**, Interaction between NAMPT and de-enveloped HSV-1 virions analysed by co-sedimentation in sucrose gradient

ultracentrifugation and immunoblotting with indicated antibodies using pelleted virions. **g**, Scatter plots of viral proteins identified by mass spectrometry after NAMPT–APEX2-mediated proximity ligation and normalization to the APEX2 control with a cutoff of >1.5-fold in the PSM numbers of viral proteins. **h**, HSV-1 proteins interact with NAMPT by co-immunoprecipitation in HSV-1-infected 293T cells that stably express FLAG–NAMPT. **i**, Immunoblotting analysis of purified HSV-1 virions derived from sgCTL and sgNAMPT HepG2 cells infected with HSV-1 (MOI = 0.1, 48 h.p.i.). Scale bar, 100 nm. Imaging data represents three (in **a**) or two (in **b**, **c** and **e**) independent experiments. PSM, peptide spectrum match.

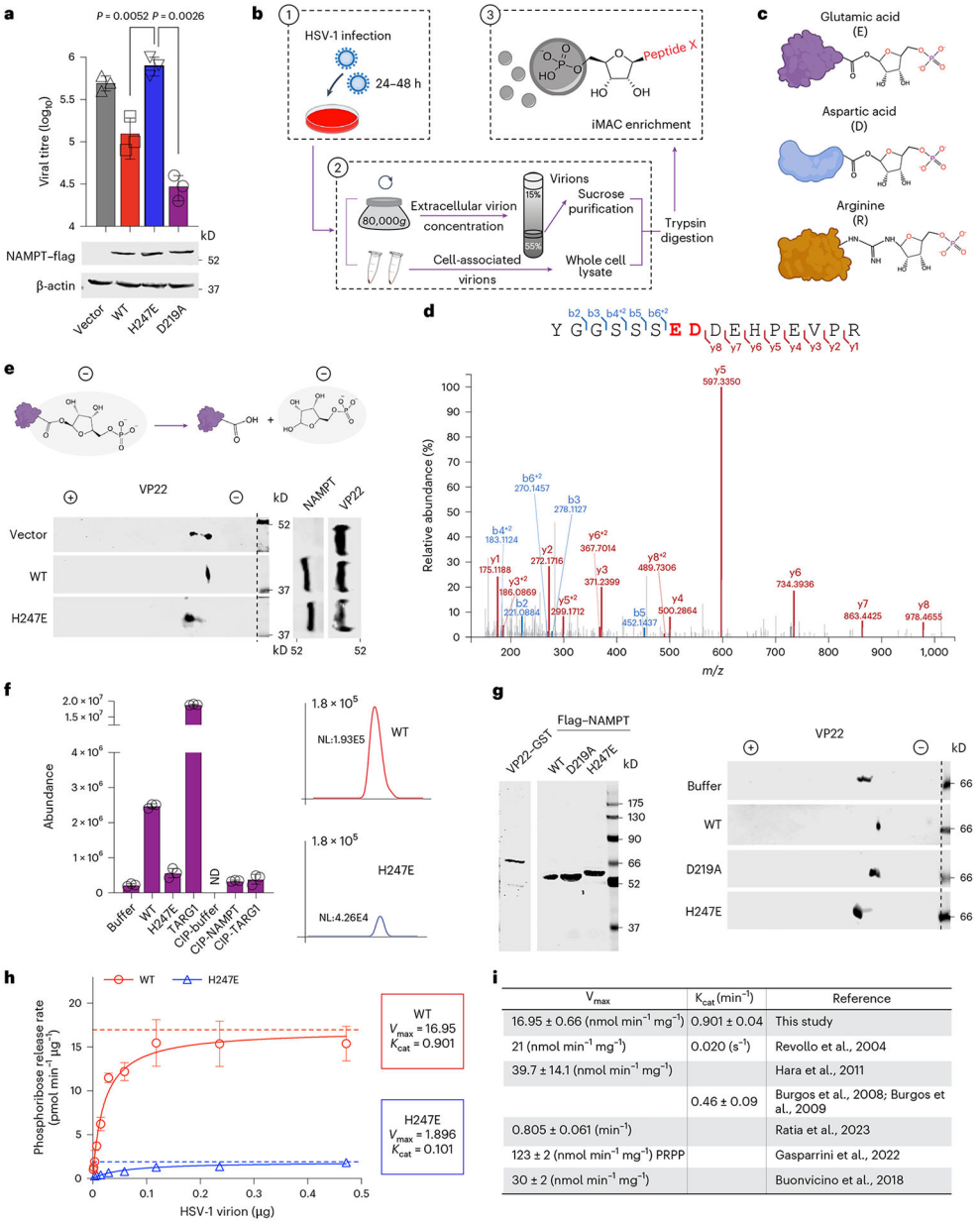

V_{max}	K_{cat} (min^{-1})	Reference
16.95 ± 0.66 (nmol min^{-1} mg^{-1})	0.901 ± 0.04	This study
21 (nmol min^{-1} mg^{-1})	0.020 (s^{-1})	Revollo et al., 2004
39.7 ± 14.1 (nmol min^{-1} mg^{-1})		Hara et al., 2011
	0.46 ± 0.09	Burgos et al., 2008; Burgos et al., 2009
0.805 ± 0.061 (min^{-1})		Ratia et al., 2023
123 ± 2 (nmol min^{-1} mg^{-1}) PRPP		Gasparrini et al., 2022
30 ± 2 (nmol min^{-1} mg^{-1})		Buonvicino et al., 2018

Fig. 4 | NAMPT is a protein phosphoribosylase.

a, HSV-1 titre in the medium of sgNAMPT HeLa cells reconstituted with wild-type (WT), H247E and D219A mutants of NAMPT at 24 h.p.i. (MOI = 0.1, $n = 3$) and whole cell lysates were analysed for the expression of NAMPT proteins (bottom panels) by immunoblotting with indicated antibodies. **b**, Schematic illustration of the procedure to identify phosphoribosylated peptides. iMAC, immobilized metal affinity chromatography. **c**, Schematic illustration of phosphoribose linked to glutamate, aspartate and arginine residues of peptides. **d**, Tandem mass spectrum of the VP22 peptide containing phosphoribosylated E74 and D75 (highlighted in red). **e**, Two-dimensional gel electrophoresis and immunoblotting analysis of 293T cells expressing V5–VP22 with WT or the H247E mutant of NAMPT. **f**,**g**, Elution profile by liquid chromatography (**f**) of

phosphoribose cleaved by NAMPT ($n = 3$), and two-dimensional gel electrophoresis and immunoblotting analysis of GST–VP22 (**g**) of the in vitro phosphoribosylase reaction. **h**, The phosphoribosylase activity of NAMPT and NAMPT-H247E was determined by an in vitro reaction containing purified HSV-1 virions and NAMPT proteins, in which the released phosphoribose was quantitatively determined by LC–MS, $n = 3$ for WT NAMPT reaction with 0.00092 μg and 0.029482 μg virion; $n = 4$ for WT NAMPT reaction with 0.0018 μg and 0.059 μg virion; $n = 5$ for WT NAMPT reaction with 0.118 μg virion; $n = 7$ for the rest of the WT groups; $n = 5$ for all H247E groups. **i**, The V_{max}, K_{cat} and K_m of NAMPT phosphoribosylase activity determined in this study compared to its phosphoribosyltransferase activity (in NMN synthesis) defined by previous studies. Statistical significance was calculated using unpaired two-tailed *t*-tests. Data in **a**, **f** and **h** are presented as mean values ± s.d. Graphics created with BioRender.com.

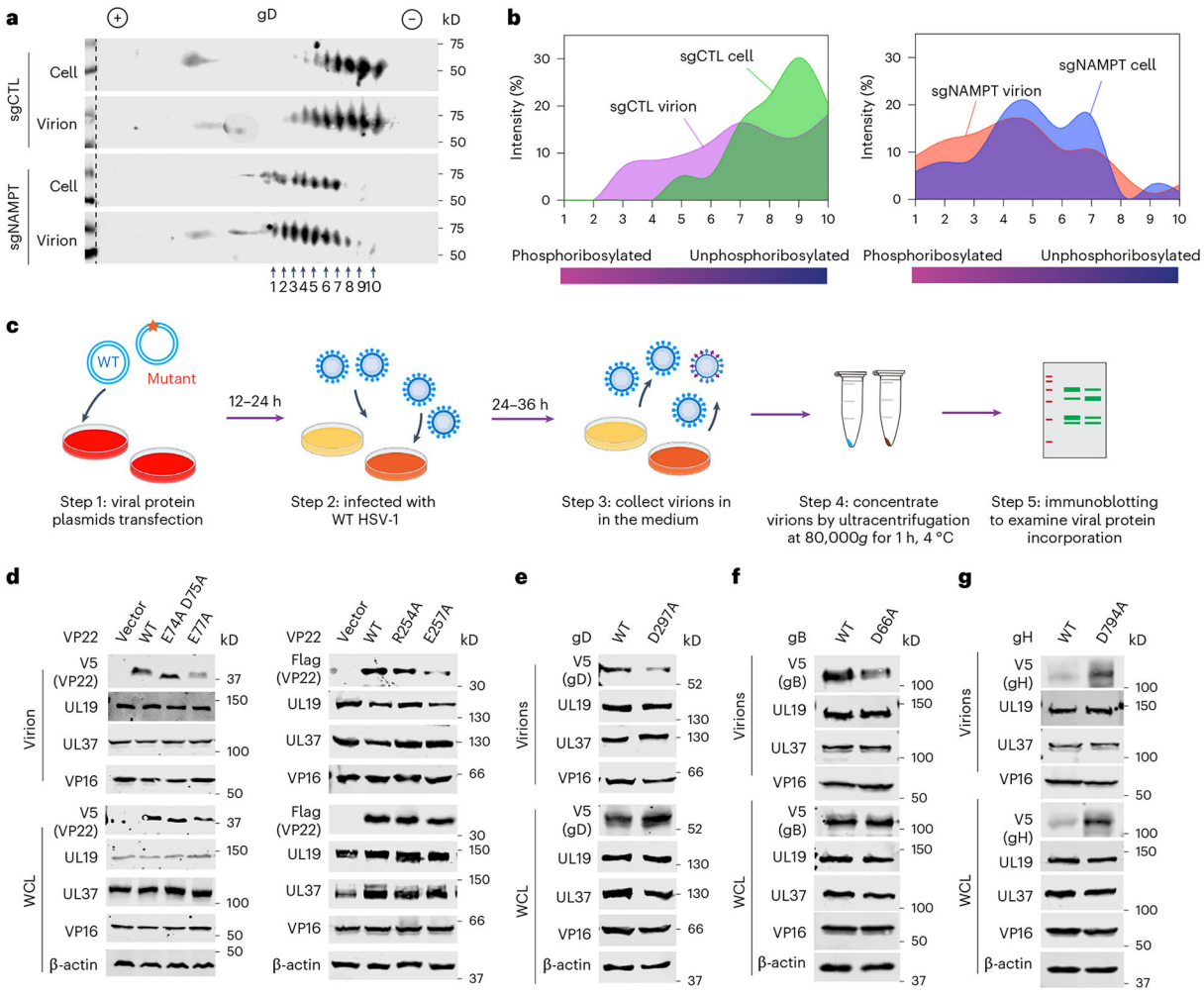

Fig. 5 |. Phosphoribose of HSV-1 structural proteins promotes their virion incorporation.

a,**b**, Two-dimensional gel electrophoresis and immunoblotting analysis of purified HSV-1 virions with antibody to gD (**a**), and quantification by densitometry of the gD species with distinct charge as indicated by arrows in (**b**). **c**, Schematic illustration of the procedure to evaluate the virion incorporation of HSV-1 mutant proteins: 293T cells transiently expressing HSV-1 proteins (WT and phosphoribosylation-resistant mutants) were infected with HSV-1 (MOI = 0.2) and extracellular virions were collected 36 h post infection for immunoblotting analysis to examine HSV-1 structural proteins in reference to their expression in 293T cells. **d**–**g**, WT and phosphoribosylation-resistant mutants of HSV-1 proteins, including VP22 (**d**), gD (**e**), gB (**f**) and gH (**g**), in HSV-1 virions and expressed in HSV-1-infected cells were analysed by immunoblotting with indicated antibodies. All HSV-1 proteins were tagged with the V5 or FLAG epitope. Graphics created with BioRender.com.

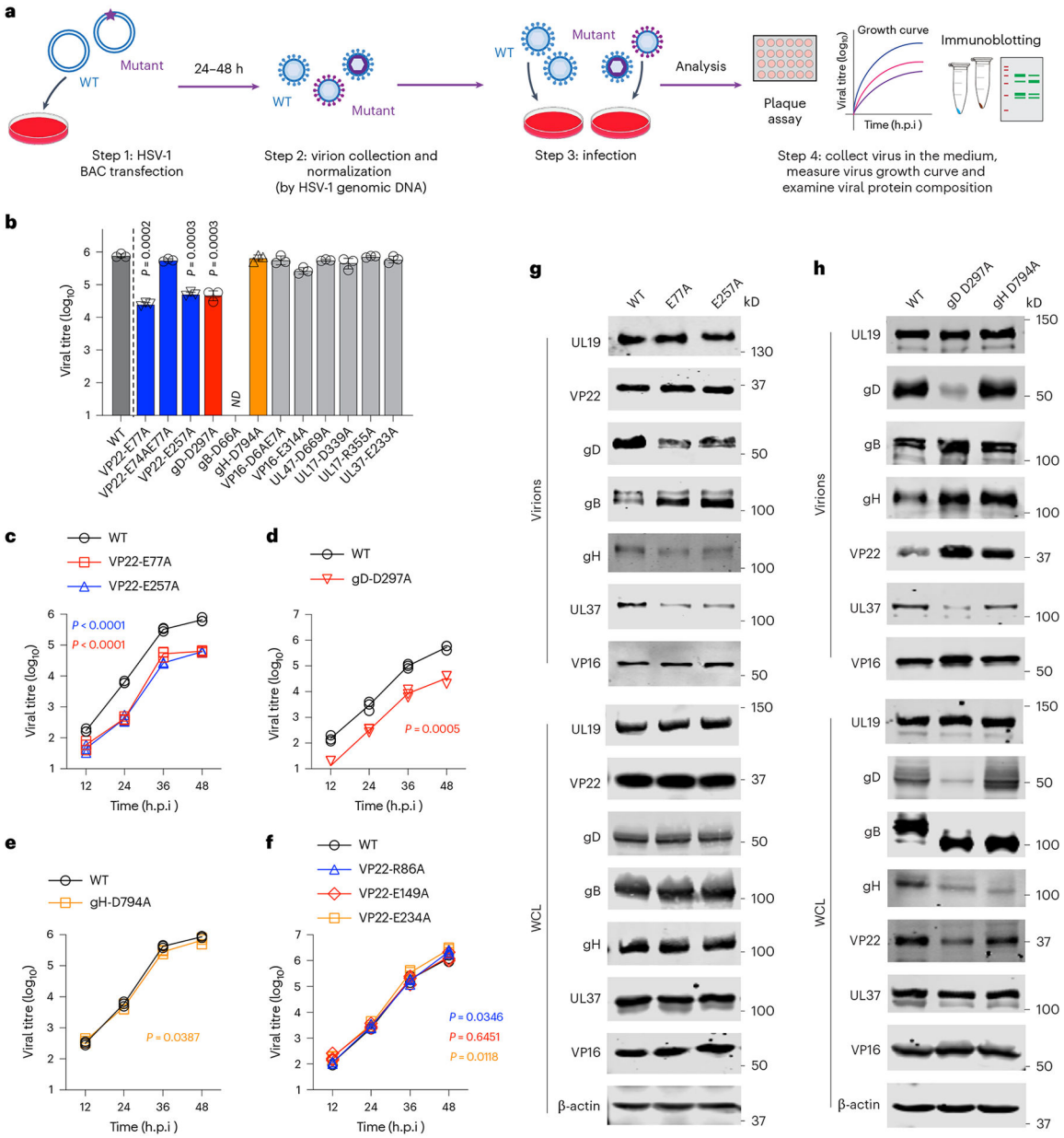

Fig. 6 | Phosphoribose of structural proteins is important for HSV-1 replication.

a, Schematic illustration of engineering and characterizing recombinant HSV-1 using BAC. **b**, Titre of recombinant HSV-1 carrying indicated mutations in the medium of HepG2 cells at 48 h.p.i. (MOI = 0.1, $n = 3$). Note, recombinant HSV-1 carrying gB-D66A failed to amplify. ND, not detected. VP22-E77A versus WT, $P = 0.0002$; VP22-E257A versus WT, $P = 0.0003$; gD-297A versus WT, $P = 0.0003$. Data are presented as mean values; error bars, s.d. **c**–**f**, Growth curve of WT HSV-1 and that containing VP22-E77A or VP22-E257A (phosphoribosylation-resistant) (**c**), gD-D297A (**d**), gH-D794A (**e**) and that containing VP22-R86A, VP22-E149A, VP22-E234A (ADP-ribosylation-resistant) (**f**) in the medium of HepG2 cells at a MOI = 0.1 were determined by plaque assay using Vero cells. **g**–**h**, Immunoblotting analysis of purified virions of recombinant HSV-1 containing VP22-E77A

or VP22-E257A (**g**), gD-D297A or gH-D794A (**h**) compared to WT HSV-1, with HSV-1 virion normalized to UL19 and whole cell lysates of HSV-1-infected HeLa cells as controls with indicated antibodies. Statistical significance was calculated using unpaired two-tailed *t*-tests for **b**; two-way ANOVA for **c**, **d**, **e** and **f**. Graphics created with BioRender.com.

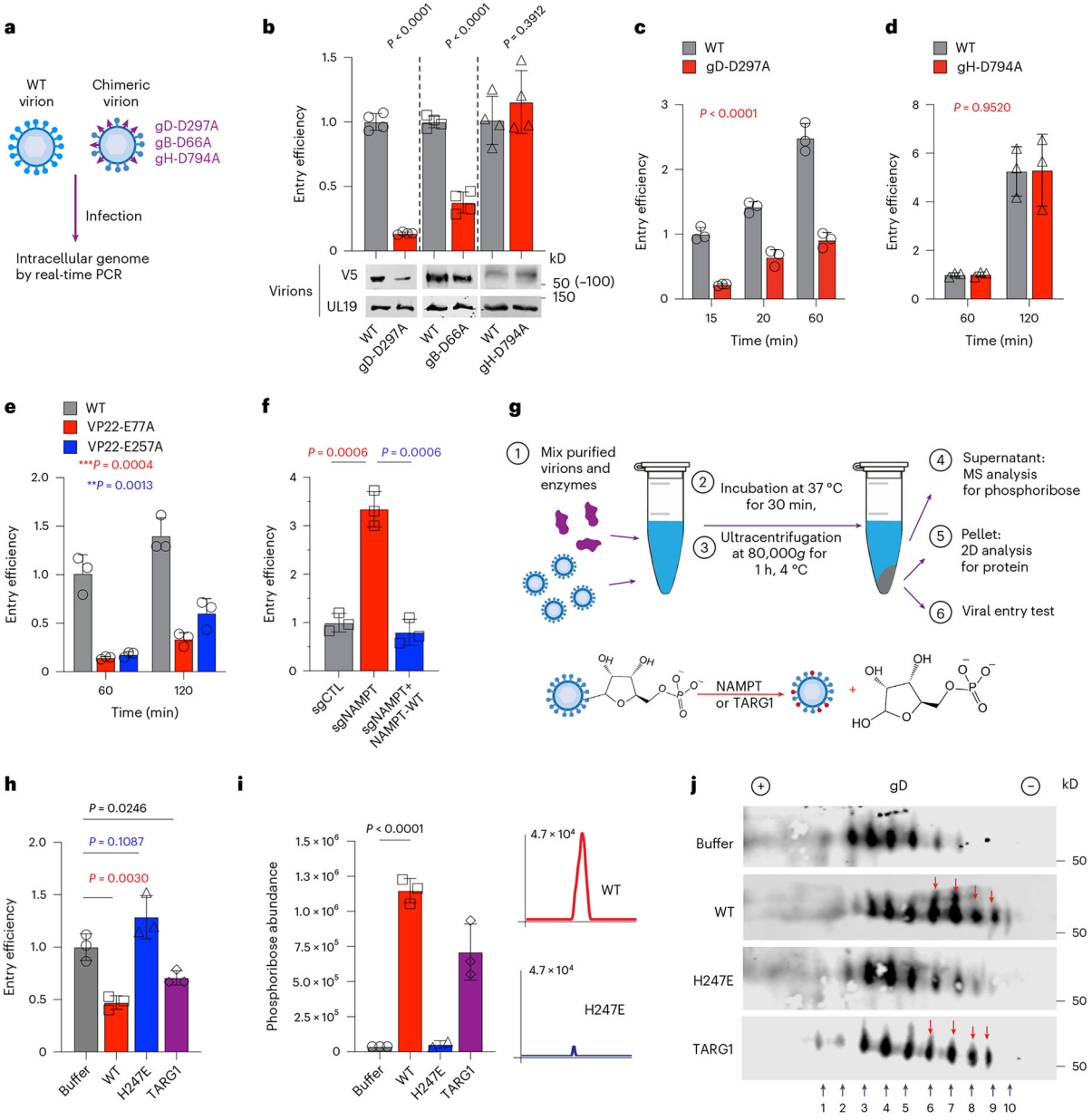

Fig. 7 | Phosphoribose of structural proteins promotes HSV-1 entry.

a, Schematic illustration of entry analysis using WT and chimeric HSV-1 virions containing gD-D297A, gB-D66A or gH-D794A. **b**, Entry analysis of HSV-1 using HeLa cells as target cells, with HSV-1 produced from 293T cells transiently expressing WT gD ($n = 4$, $P < 0.0001$), gB ($n = 4$, $P < 0.0001$) and gH or their corresponding phosphoribosylation-resistant mutants as indicated. **c**–**e**, Entry analysis of WT recombinant HSV-1 and that containing VP22-E77A or VP22-E257A mutations; $n = 3$, $P = 0.0004$ for VP22-E77A versus WT, $P = 0.0013$ for VP22-E257A versus WT (**c**), gD-D297A, $n = 3$, $P < 0.0001$ (**d**) or gH-D794A, $n = 3$, $P = 0.9520$ (**e**). **f**, Entry analysis of HSV-1 produced from sgCTL, sgNAMPT HeLa cells, or sgNAMPT HeLa cells reconstituted with NAMPT; sgNAMPT versus sgCTL, $n = 3$, $P = 0.0006$; sgNAMPT + WT versus sgCTL, $P = 0.0006$. **g**–**j**, Schematic illustration of

the in vitro phosphoribosylase reaction and subsequent functional or biochemical analysis using purified HSV-1 virions (**g**). Entry analysis (WT versus buffer, $n = 3$, $P = 0.003$; H247E versus WT, $P = 0.1087$; TARG1 versus buffer, $P = 0.0246$) (**h**), quantification of phosphoribose released in the phosphoribosylase reaction by mass spectrometry (WT versus buffer, $n = 3$, $P < 0.0001$) (**i**) and two-dimensional gel electrophoresis and immunoblotting analysis with anti-gD antibody of HSV-1 virions treated with NAMPT, NAMPT-H247E or TARG1 (**j**). Statistical significance was calculated using unpaired two-tailed *t*-tests, for **b**, **f**, **h** and **i**, two-way ANOVA for **c**, **d** and **e**. Data in **b**, **f**, **h** and **i** are presented as mean values; error bars, s.d.